The Journal of Neuroscience, April 1992, 12(4): 1169–1193

Neural–Vascular Relationships in Central Retina of Macaque Monkeys (*Macaca fascicularis*)

D. Max Snodderly,[1,2,3] Richard S. Weinhaus,[1,2,a] and John C. Choi[1,b]

[1]Neuroscience Unit, Eye Research Institute, Boston, Massachusetts 02114 and [2]Department of Ophthalmology and [3]Program in Neuroscience, Harvard Medical School, Boston, Massachusetts 02115

The relationship of the vasculature to the neuronal layers was studied in whole-mounts and in sections of macaque retinas. Like other central nervous structures, primate retinas have local variations in vascularity that reflect local variations in metabolism, rather than simply tissue thickness or volume. A special feature of the retina is a dense vascular plexus in the nerve fiber layer, which is unmyelinated and hence must generate a substantial metabolic demand for ion pumping.

Much of the retinal vasculature is laminated and located at specific layer boundaries. Throughout the central retina, two planes of capillaries bracket the inner nuclear layer to form a sclerad capillary network. In some regions, especially near the fovea, a second, more vitread network brackets the ganglion cell layer with another pair of capillary planes. Wherever the nerve fiber layer is thick, the vitread network becomes less planar and is multilayered. When surrounded by nerve fibers, capillaries tend to orient parallel to the fibers; when adjacent to ganglion cell bodies, the capillaries are less systematically oriented. At the border between the nerve fiber layer and the ganglion cell layer, rows of ganglion cells often interdigitate with nerve fiber bundles, resulting in local perturbations of capillary orientation.

The volume of the sclerad capillary network is relatively constant at different locations, but the volume of the vitread network increases dramatically where the nerve fiber layer is thick. As a result, the vascularity of the retina is greatest in the peripapillary region near the optic disk, even though the total thickness of the peripapillary retina is comparable to the retinal thickness near the foveal crest. As many as 60–70% of the photons passing through the retina in the peripapillary region will encounter one or more capillaries before reaching a photoreceptor.

Median capillary diameter increases with retinal depth from 4.5–4.7 μm in the nerve fiber layer to 5.0 μm at the sclerad border of the inner nuclear layer. Capillary diameter in the nerve fiber layer also increases near the optic disk.

Within the central retina of diurnal primates, the topographic variations in the neuronal layers create large differences in the proportions of the cellular elements at different retinal loci. In the center of the fovea, the retina is thin and only photoreceptors are present. At the foveal crest, the ganglion cell layer reaches its greatest thickness, but the optic nerve fiber layer is very thin. In the vicinity of the optic disk, the ganglion cell layer is thin, but the nerve fiber layer is thick. The total thickness of the retina is a combined function of these widely varying component layers.

It has long been appreciated that the thickness of the retina is one determinant of its vascularity (Michaelson, 1954; Chase, 1982; Buttery et al., 1991). If the retina is thin (as in the foveal center), the oxygen demand can be met by diffusion from the choroidal circulation, but in more eccentric loci where the retina is thicker, an intraretinal blood supply with multiple layers becomes prominent (Michaelson, 1954; Shimizu and Ujiie, 1978; Snodderly and Weinhaus, 1990).

The spatial distribution of the vascular network of primate retinas, including humans, has been the subject of surprizingly little quantitative study. This is partly due to conflicting conclusions from earlier work (Michaelson, 1954; Toussaint et al., 1961; Wise et al., 1971; Shimizu and Ujiie, 1978) about the relationships between the retinal capillary networks and the neuronal layers. Without a clear understanding of the neural–vascular relationships, it is difficult to account for the large regional variations in the vasculature.

More recent work has shown an intricate and precise relationship between the retinal capillary networks and the neuronal layers in the foveal region. In human retinas the capillaries of the ganglion cell layer are located at a border or in the middle of the layer, depending on the retinal eccentricity and the thickness of the layer (Iwasaki and Inomata, 1986). Within the foveal depression of squirrel monkeys, we have identified four distinct capillary planes that are located near the borders of the inner nuclear layer and the ganglion cell layer (Snodderly and Weinhaus, 1990). With increasing eccentricity, the most superficial (i.e., most vitread) capillary plane moves into the nerve fiber layer. As a result of this arrangement, the capillary planes are appropriately located near regions of high metabolic demand as indicated by the cytochrome oxidase distribution (Kageyama and Wong-Riley, 1984).

In the present article, we extend our analysis of neural–vas-

Received June 7, 1991; revised Oct. 28, 1991; accepted Nov. 5, 1991.

This work was supported by NIH Grants EY06591 and T32 EY07074. Printing costs for the color plate were partially defrayed by a donation from Allergan Pharmaceuticals. Marita Mullan-Sandstrom and Richard I. Land, Jr. provided expert technical assistance. James D. Broderick constructed the drawings of peripapillary regions P1–P4. Dr. Margaret S. Livingstone generously donated retinal tissue. John C. Choi submitted portions of this work as an honors thesis at Harvard Medical School.

Correspondence should be addressed to D. Max Snodderly, Neuroscience Unit, Eye Research Institute, 20 Staniford Street, Boston, MA 02114.

[a] Present addresses: Eye Research Institute, Visual Services, Harvard Community Health Plan, and General Eye Service of Massachusetts Eye and Ear Infirmary.

[b] Present address: Department of Ophthalmology, University of Southern California, Los Angeles, CA 90033.

cular relationships to additional loci within the central retina, including the peripapillary region around the optic disk. We have chosen macaque retinas for this study because of the similarity of their vasculature to that of human retinas (Henkind, 1967; Anderson, 1971; D. M. Snodderly and R. S. Weinhaus, unpublished observations). Our results show that the nerve fiber layer contributes more to retinal vascularity than would be predicted from its contribution to total retinal thickness. This finding suggests that retinal vascularity, like the vascularity of other central nervous structures, is more strongly related to local metabolic activity than to tissue volume (Borowsky and Collins, 1989; Zheng et al., 1991).

Materials and Methods

Cynomolgous monkeys (*Macaca fascicularis*), imported primarily from the Phillipines, were used. Retinas were coded by species (F for *fascicularis*), a two-digit identification number, and right (R) or left (L) eye. Four retinas from three monkeys were studied intensively in whole-mounts, and measurements of the vascular network and the thickness of the neuronal layers were made. The sex and weight at the time of death of these three animals were as follows: F22: female, 2.9 kg; F46: male, 2.8 kg; F54: male, 2.9 kg. In addition, retinal whole-mounts from three other animals (F04, F48, and F53) and serial sections from retinas of five animals (F01, F04, F10, F22, and F48) were studied to confirm the generality of the patterns observed.

Preparation of retinal tissue

The methods for preparation of retinal tissue have been published (Snodderly and Weinhaus, 1990) and will only be described briefly here along with subsequent modifications. Monkeys were killed by injection of an overdose of sodium pentobarbital. The intensively studied retinas were from animals whose retinas were then immediately fixed by transcardial perfusion of the animal with 0.9% sodium chloride containing 0.5% sodium nitrite followed by half-strength Karnovsky's fixative (2% paraformaldehyde and 2.5% glutaraldehyde in 0.1 M phosphate buffer, pH 7.2–7.4). Less intensively studied retinas were fixed with slight variations in the saline prewash and the fixative composition.

The eyes were enucleated, opened at the pars plana, and postfixed in half-strength Karnovsky's fixative for an additional 2–24 hr. After removal of the vitreous, an 8 × 10 mm posterior segment was cut from the globe that extended superiorly, inferiorly, and temporally for at least 3.5 mm from the foveal center and for at least 0.5 mm beyond the nasal margin of the disk. This central segment of the globe was placed in 0.1 M phosphate buffer. To separate the retina from the choroid and sclera, the optic nerve fibers were gently severed at the level of the lamina choroidalis with a microsurgical spatula. The retina was then freeze-protected by transfer to increasing concentrations of glycerol (12.5%, 25%, and 50%) in buffer.

At this stage, the pigment epithelium was still adherent to the retina. Total retinal thickness of two retinas (F46R and F54R) was measured as described below, before dissecting off the pigment epithelium. All other retinas were immediately dissected further to optimize visualization of intraretinal features. The pigment epithelium was removed by freezing the retina and scraping off the melanin-containing tissue (Snodderly and Weinhaus, 1990).

For microscopic study, the tissue was placed vitread side up in a shallow well 275–375 μm deep and coverslipped (Snodderly and Weinhaus, 1990). The well was filled with 50% glycerol in buffer, with sodium azide (0.04% or 0.08%) added as a preservative. Even with the added azide, small particles, presumably microorganisms, could be observed moving in the liquid phase after several months. When this occurred, the tissue was dismounted, soaked in fixative for several hours to disinfect it, rinsed in buffer, and remounted.

Whole-mounts were stored at −80°C to −90°C except when being studied. Despite repeated cycles of freezing and thawing, the capillary network and the neuronal layers were clearly visible for periods greater than 18 months. Slow evaporation of the fluid in the well caused gradual deterioration in the visibility of retinal features. When the retina was remounted in a fresh solution, however, the initial clarity was restored.

To confirm that the microscopic images of the retinal whole-mount permitted accurate localization of the retinal capillary planes in relation to the neuronal layers, portions of selected whole-mounted retinas were dismounted and serial sections 40 μm thick were prepared (Snodderly and Weinhaus, 1990).

Drawings

The vasculature in whole-mounts was drawn by using drawing tubes mounted on an Olympus BHS microscope with a viewing magnification of 330× or a Zeiss UEM microscope at 256× magnification with standard bright-field optics. Four centimeters in the drawing plane corresponded to 100 μm on the retina. A continuity diagram of the vessels was traced by changing the focus, and the vessel segments were assigned to their respective depth planes. Ambiguous relationships were clarified at higher magnification with Nomarski differential interference contrast (DIC) optics using the Zeiss system. The DIC optics provided increased contrast and decreased depth of field.

Anatomical features visible in retinal sections were drawn with DIC optics at a magnification of 200×. In these relatively thick sections, only a single focal plane close to the coverslip was drawn so that the layer borders could be represented as single lines in a thin optical plane. When the borders were irregular, a visual average was sketched as a smooth line.

Quantitative measures of the capillary network

Quantitative measures of the capillary network were made in the retinal whole-mounts in 100 × 100 μm sampling areas. The 87 sampling regions were approximately midway between arteries and veins, at least 60 μm from major vessels, to minimize local perturbations of the capillary network.

Selection and repeated evaluation of the sampling regions were facilitated by fitting the Zeiss UEM microscope with a stage with motor control of the x- and y-axes (New England Affiliated Technologies, Lawrence, MA), and a linear encoder (Dynamics Research, Wilmington, MA) on the z-axis, so that a continuous digital display of the x, y, and z coordinates was available. The digital output of the display was recorded by a microcomputer for further analysis.

Capillary screening areas. The percentage of the retinal area covered by capillaries was estimated after enlarging the drawing of each 100 × 100 μm sampling area to a square 10 × 10 cm. The area devoid of vessel profiles was measured with a Zeiss Videoplan digitizing system and subtracted from the total area to derive the retinal area optically screened by one or more capillaries.

Capillary lengths, diameters, and volumes. Lengths of capillary segments in the x–y plane were measured from drawings using the Videoplan digitizing system. Diameters of capillary lumens were directly measured at the microscope with DIC imaging at 800× magnification by superimposing the image of the capillary in the whole-mount on a scale imaged through the drawing tube. For each segment, the mean of diameters measured at three locations distributed along the segment was recorded.

Volume estimates were calculated as the product of the capillary segment length and its cross-sectional area, assuming a cylindrical shape with a circular cross section of uniform diameter. To verify that treatment as a uniform cylinder was realistic, the diameters of more than 70 capillary segments of F46R and F54R were measured at locations all the way from the arterial to the venous end of the segment. No consistent trends in diameter along the segments were found. Individual segment volumes were summed to obtain estimates of total capillary volume in each capillary grouping. Our complete sample included 1628 capillary segments.

Because our measurements of capillary segment lengths were made from two-dimensional maps in the x–y plane, and do not incorporate any vertical component, the derived volumes are underestimates. To assess the error involved, we measured at the microscope the vertical (z) component of length for each capillary segment in a subset of the sampling areas. The hypotenuse of the length in the x–y plane and the orthogonal component in the z-axis were then calculated to obtain an improved estimate of capillary segment length and volume. The results showed that we underestimated capillary volume by an average of 7% in the peripapillary region and 3% in other sampling areas. No corrections have been made for these small errors.

Measurement of retinal thickness and neuronal layer thicknesses

For two retinas (F46R and F54R), total retinal thickness and the thickness of the outer retina were measured in whole-mounts before removal

of the pigment epithelium. Thickness measurements were made by focusing through the tissue with a 40× water-immersion objective. The total thickness was estimated as the distance between the planes of best focus of the inner limiting membrane and of the vitread border of the retinal pigment epithelium. Here the epithelial cell mosaic was visible and melanin granules first came into sharp focus. For macaque retinas, the uppermost pigment granules are about 8 μm from Bruch's membrane, the boundary at which the retina usually separates from the choroid in our dissections. Control measurements were done on one retina whose thickness was first measured in whole-mount and then remeasured in a side view of a slice cut from the retina with a razor blade. Thickness values obtained from the whole-mount were about 12% less than those measured from the side view. This discrepancy is too small to affect our conclusions, and no correction has been applied to the data.

The thickness of the outer retina was measured as the distance from the capillary plane at the deep (sclerad) border of the inner nuclear layer to the vitread border of the pigment epithelium.

For the other two whole-mounts from which quantitative data were obtained (F22R and F22L), most of the pigment epithelium was dissected off immediately so that only small extrafoveal patches remained. In these retinas, when a sampling area was near a patch of pigment epithelium, a measurement of outer retinal thickness from the region of the patch was used. For sampling areas in the foveal region, where all pigment epithelium was removed, an estimate of outer retinal thickness was used by taking an average of measurements at comparable loci from F46R and F54R. Values for total retinal thickness of F22R and F22L were derived by adding the thickness of the outer retina estimated in this way to the measured thickness of the inner retina.

With the pigment epithelium removed, the thickness of each layer of the inner retina was measured for each 100 × 100 μm sampling area for all retinas. In sampling areas where the ganglion cell/nerve fiber boundary was irregular (a common occurrence), an average of the values at several locations was used.

Results

Laminar distribution of the vasculature

For each retinal whole-mount, a photographic montage or a drawing was prepared to construct a map of the large vessels, the foveal avascular zone, and the optic disk for use as landmarks (Fig. 1). Subsequent figures refer to these maps to illustrate topographic relationships.

In this article, we have concentrated on the central retina, which we define as the approximately circular region centered on the fovea and extending along the vertical meridian to include the superior and inferior temporal retinal arteries (Fine and Yanoff, 1979). On the horizontal meridian, we have studied the retina as far nasally from the fovea as the optic disk and for an equal distance temporally.

The organization of the vascular network of the macaque fovea is similar to that already described for the squirrel monkey (Snodderly and Weinhaus, 1990). In the whole-mounts, the vessel lumens appear as interconnecting tubes differing in contrast from the surrounding retinal tissue (Snodderly and Weinhaus, 1990). Radially oriented arteries and veins in the ganglion cell layer are connected by capillaries that are located at preferred tissue planes. Four planes of capillaries can be recognized at many locations. Because of their different characteristics, we will divide these four planes into two groups, a sclerad network that brackets the inner nuclear layer, and a vitread network that brackets the ganglion cell layer or lies within the ganglion cell and nerve fiber layers (Fig. 2).

In our illustrations and our terminology, we have adopted the convention that the retina is oriented vitreous surface up, photoreceptors down. Thus, the terms "shallow," "superficial," and "vitread" mean a common direction in space, opposite to "deep" and "sclerad." This convention facilitates *in vivo/in vitro* comparisons, since the retina is usually viewed *in vivo* with the vitreous surface toward the observer, so that objects deeper in the retina are more sclerad.

Sclerad network

Throughout the central retina, capillaries at both borders of the inner nuclear layer are visible as planar arrays in whole-mount images (Fig. 2) and in retinal sections (see below). These capillary planes, called the deep inner nuclear plane and the shallow inner nuclear plane (Snodderly and Weinhaus, 1990), form the sclerad network. Few capillaries are seen in the interior of the inner nuclear layer; in regions of the whole-mounts where cloudiness made visualization of cell bodies difficult, the boundaries of the inner nuclear layer could readily be determined by focusing on its bordering capillary planes. The only exception to this rule occurs in an annulus approximately 50–75 μm wide surrounding the foveal avascular zone; here the inner nuclear layer is relatively thin and capillaries sometimes lie within it.

Vitread network

The vitread network is also planar in some local regions (Figs. 2, 3). In the foveal region especially, the two planes of capillaries forming the vitread network tightly bracket the ganglion cell layer. Here, the retina has four strict planes of capillaries, one pair bracketing the ganglion cell layer and the other pair bracketing the inner nuclear layer [Fig. 4, 4 Planes (second photo in row 1)]. However, at greater eccentricities, the vitread network becomes less planar and it is strongly affected by retinal topography. This is illustrated in rows 2 and 3 of Figure 4, which depict a section that extends from the center of the fovea to 4 mm eccentricity. The key factors influencing the vitread network appear to be variations in the thickness of the ganglion cell and nerve fiber layers and the orientation of the nerve fiber bundles.

The border between the ganglion cell layer and the nerve fiber layer. The border between the ganglion cell layer and the nerve fiber layer is consistently nonplanar in many retinal regions where both layers are well developed. At the interface between these two layers, the ganglion cells are often arranged in irregular rows one to three cells wide that interdigitate with nerve fiber bundles (Fig. 3, upper right). This gives the border an undulating character, with small hills of ganglion cells creating valleys in which the nerve fibers run. We are not aware of a previous description of this striking retinal feature.

Vascularization of the ganglion cell layer. Within the foveal depression, a capillary plane lies at or near the deep border of the ganglion cell layer, along with the major vessels, as previously described for the squirrel monkey (Snodderly and Weinhaus, 1990). The close association of this plane of capillaries with the large vessels prompted us to use the locations of the large vessels as an aid to identify the ganglion cell capillary plane in the extrafoveal retina.

It was helpful to recognize that major vessel trunks in the vitread network lie mainly in the ganglion cell layer. To establish this fact, we studied whole-mounts of four retinas (F22L, F46R, F53R, and F54R) and confirmed the laminar relationships in sections of a fifth retina (F48R).

Medium-sized vessel trunks could be readily assigned to the appropriate neural layer. The more difficult cases were vessels sufficiently large to protrude into more than one layer and those with an asymmetric cross section. The large veins in particular often have obviously noncircular or asymmetric cross sections. In the whole-mounts, asymmetry was evident when the focal planes for the bottom and the top surfaces of the vessels were

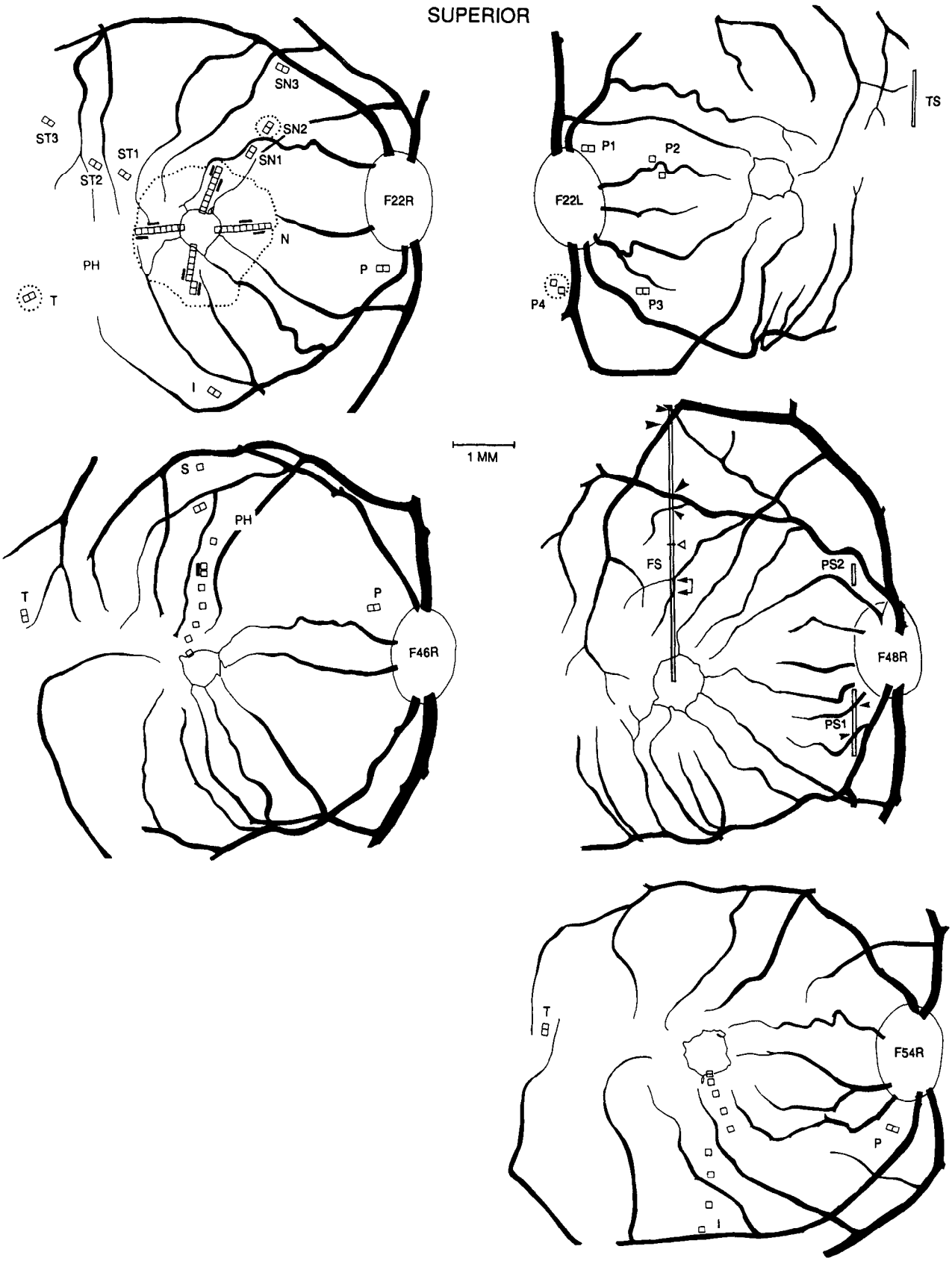

Figure 1. Retinal regions where the vasculature was illustrated or quantitatively measured. Selected large vessels, the foveal avascular zone surrounded by the terminal capillaries, the outlines of the optic disks, and the animals' identification numbers are shown. The retinas are oriented according to standard fundus photographic convention, with the optic disk on the nasal side. The complete vascular networks within the *dotted regions* of F22R and F22L are displayed in Figure 5. *Sampling areas. Small squares* indicate the 100 × 100 μm sampling areas within which

not equidistant from the focal plane where the trunk was widest. For the example shown in Figure 3 (left column), the widest part of the trunk of the large vein was about three times as far from the bottom surface of the vein as it was from the top surface. Departures from roundness of the large vessels are also implied by the oblong profiles visible in sections orthogonal to the vessel axes (Fig. 4). Other examples can be seen in Wise et al. (1971), their Figures 2-6 and 3-2, and Shimizu and Ujiie (1978), their Figures 17, 36, 98, and 103.

To be consistent, we assigned all major vessels to the lamina where their trunk was widest. The pattern derived with this criterion is relatively simple: when the optic nerve fiber layer was thick, near the optic disk, the major vessels were in the nerve fiber layer [see Fig. 4, Thick NF (row 4)]. As the major vessels moved away from the edge of the disk, they descended into the ganglion cell layer within 0.5 mm, with one exception, an artery that traveled for 0.8 mm before descending to the ganglion cell layer. The only other cases where major vessels were displaced from the ganglion cell layer occurred where veins and arteries crossed each other. For example, such displacements occurred routinely where venous tributaries crossed the superior and inferior temporal retinal arteries. Even there, the vessel trunks returned to the ganglion cell layer within 0.2 mm of the crossings.

Where the large vessels are in the ganglion cell layer, the most prominent capillary plane in the ganglion cell layer is at about the same retinal depth as the large vessels. This capillary plane is distinct from the nerve fiber capillary grouping above it in three ways: (1) it is present throughout the entire central retina including the fovea, except for the foveal avascular zone and a surrounding annulus 50–70 μm wide; (2) its capillaries are often not parallel to the nerve fiber bundles; and (3) it is present in extrafoveal regions where the nerve fiber layer is thin or indistinguishable [Fig. 4, Temporal section, TS (row 4)].

With increasing retinal eccentricity outside the fovea, the ganglion cell capillary plane gradually migrates vitread relative to the ganglion cell layer boundaries. This change of position occurs as the cell layer becomes thinner and the overlying nerve fiber layer thickens. Out to an eccentricity of about 1.3 mm, the capillaries lie near the deep border of the ganglion cell layer. Along the foveal plateau from about 1.3 to 1.7 mm eccentricity, they are often in the interior of the cell layer. At greater eccentricities, from about 1.7 to 2.5 mm, they are more frequently located near the shallow (vitread) border of the cell layer. At eccentricities greater than about 2.5 mm, the ganglion cell layer thins to two cells or less in thickness, and the capillaries can intermittently touch either the deep or shallow border of the cell layer. They tend to lie closer to the shallow border wherever the overlying nerve fiber layer is thicker than about 5 μm.

All capillaries having the characteristics described above were assigned to the ganglion cell plane (Fig. 2) and were coded in the same color in our continuity maps of the vasculature (Fig. 5). Where this principal plane was superficial (vitread) to the deep border of the ganglion cell layer, there were sometimes a few additional capillaries at the deep border of the cell layer. They were also assigned to the same ganglion cell network.

The capillary plexus of the nerve fiber layer. Capillaries near the border between the ganglion cell and nerve fiber layers can be sandwiched between cell bodies and nerve fiber bundles, surrounded by cell bodies, or surrounded by fiber bundles. If they are surrounded by fiber bundles, the long capillary segments orient mainly parallel to the bundles (Figs. 2, top; 3, lower right). Slightly deeper capillary segments sandwiched between fiber bundles and cell bodies at the bottoms of the border valleys are often not parallel to the fibers. Shorter interconnecting segments between neighboring capillaries or between capillaries and major vessels can be oriented diagonal or orthogonal to the fiber bundles.

In terms of their physiological function, the capillaries in this border region must supply nutrients to both the ganglion cell and nerve fiber layers since the diffusion distances are short. Furthermore, because nerve fibers initially travel through the ganglion cell layer before entering the nerve fiber layer proper, they too are served by capillaries in the superficial part of the ganglion cell layer.

Without implying that they supply the nerve fibers *exclusively*, we have assigned capillaries to the nerve fiber capillary plexus on the basis of the following anatomical characteristics: (1) they are located superficial to the principal capillary plane of the ganglion cell layer, either within the nerve fiber layer or near the ganglion cell/nerve fiber layer boundary; (2) long segments are parallel to the nerve fibers except when connecting to major vessels or when adjacent to ganglion cells; and (3) these capillaries are infrequent or absent where the nerve fiber layer is thin, especially temporal to the fovea near the horizontal raphe (Fig. 4, Temporal section, TS). One consequence of using these criteria is that occasional capillaries within the superficial portion of the ganglion cell layer are assigned to the nerve fiber plexus—primarily within an annulus from about 0.7 mm to 1 mm retinal eccentricity where the ganglion cell layer is very thick. This has little effect on our measurements of capillary volumes because the contribution of these few capillaries is quantitatively minor compared to the dense network that is unambiguously within the nerve fiber layer (see below).

The capillaries in the nerve fiber layer are not organized in planes like those of the sclerad network bracketing the inner nuclear layer. As the nerve fiber layer builds up toward the disk, we have observed as many as eight overlying "layers" of nerve fiber capillaries. The progressive addition of capillaries as the nerve fiber layer thickens is illustrated in photographs and drawings of retinal sections in Figure 4. The nerve fiber capillaries form a three-dimensional plexus, with long, horizontal capillary segments connected by short vertical or oblique segments, as previously described by Shimizu and Ujiie (1978).

As the three-dimensional plexus becomes more and more elaborate, some of the complex features that can be observed

←

capillary parameters were quantitatively measured. Data from adjacent sampling areas with bars alongside them were averaged together. Locations of the sampling regions are coded by the abbreviations *I*, inferior; *N*, nasal; *S*, superior; *SN*, superonasal; *ST*, superotemporal; *T*, temporal; and *P*, peripapillary. *Photographic locations.* For Figures 2 and 3, photographs of *F22R* were taken at sampling locations *SN1* and *SN2*; additional photos, but no measurements, were taken at locations *PH* in retinas *F22R* and *F46R*. *Section locations.* The locations and the orientation of retinal sections illustrated in Figure 4 are indicated by *narrow vertical rectangles*, a temporal one (*TS*) from the upper right corner of F22L, and foveal (*FS*) and peripapillary ones (*PS1* and *PS2*) from *F48R*. *Arrowheads* point to major vessels that are similarly identified in the drawings in Figure 4. The *open triangle* just above the label *FS* demarcates where the drawing of the foveal section in Figure 4 was divided to fit the page.

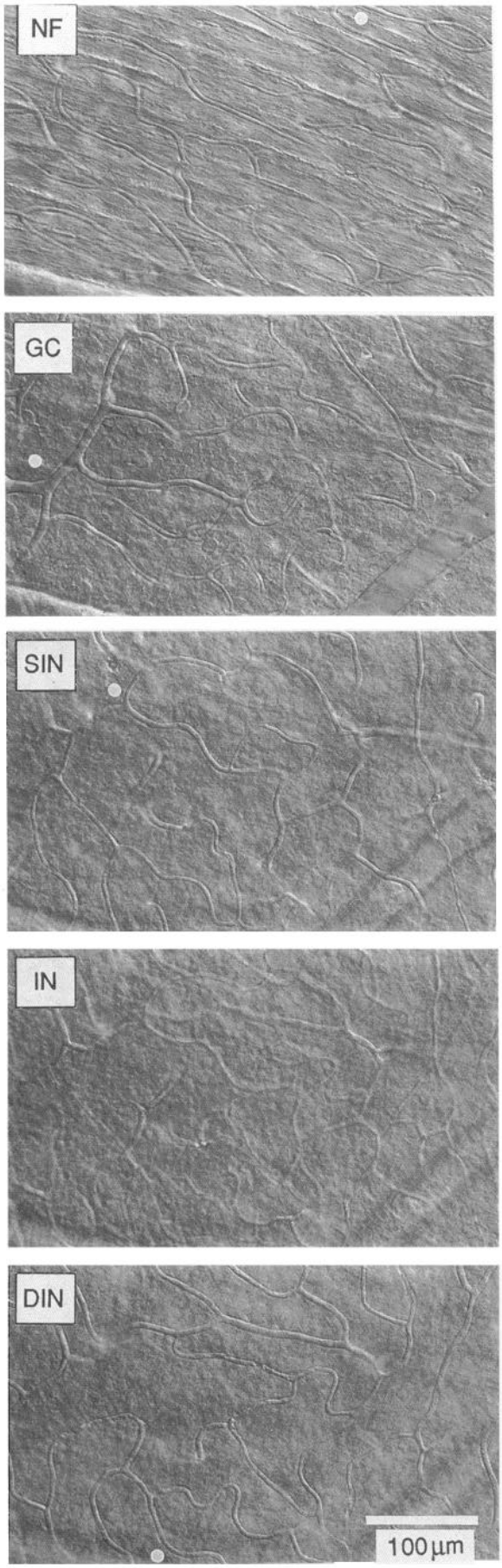

in the horizontal (tangential) plane can also be found oriented in the orthogonal plane (vertically). For example, compare the horizontally oriented loop in the whole-mount view in the top right corner of the top panel of Figure 2 with the vertically oriented loop in the third photo of Figure 4.

Vascular connections and topography

By successively focusing through the whole-mounts, one can visualize the relationships among the planes of capillaries and the neuronal layers. Only a fragmentary picture of the relationships can be obtained photographically, however, because the capillaries interconnect by vertical segments and because the tissue planes are parallel to the focal plane of the microscope only over short distances. This can be appreciated by comparing the photographs in Figure 2 with the continuity diagram of the same region (SN2) in the upper right corner of Figure 5. Consequently, the continuity diagrams form the basis for our analyses.

The central portion of Figure 5 is a continuity diagram of the complete vascular network of a fovea and its surround. It illustrates the dramatic changes in the capillary network that occur as the inner retina thickens in the foveal region. At the corners of the figure are continuity diagrams of complete vascular networks of three extrafoveal regions with different thicknesses of the nerve fiber layer (P4 > SN2 > T). These diagrams give a visual impression of the influence of the nerve fiber layer on retinal vascularity.

At the bottom of the foveal map near V4, and in the superonasal region SN2, two layers of nerve fiber capillaries are present. This type of layering is illustrated in retinal sections in Figure 4 (upper left corner, under the inverted open triangle). For visual clarity, we coded these two vessel layers in different colors in Figure 5. We continued to use only two colors to code the more elaborate capillary plexus in the nerve fiber layer of the peripapillary region (P4). The layer of nerve fiber capillaries (NF) closest to the ganglion cell capillaries is coded in yellow, and *all* more superficial capillaries are coded in red (NFs). This is intended to illustrate the great proliferation of the more superficial capillaries in retinal regions with a thicker nerve fiber layer.

With a magnifying glass, more details of the interconnections of the vascular networks can be seen. For readers wishing to study the geometry of the possible blood flow paths, we can provide a larger color print of this figure at a reasonable cost.

The foveal region

The foveal vascular network of the macaque retina is similar in many respects to that of the squirrel monkey described previously (Snodderly and Weinhaus, 1990). Figure 5 covers a greater retinal expanse than our earlier drawing of a squirrel monkey fovea, so more of the foveal crest and the surrounding plateau is included.

←

Figure 2. Photographs with DIC optics of the principal capillary planes in the whole-mount of retina F22R at location SN2 (2 mm eccentricity) indicated in Figure 1. Capillary networks in the nerve fiber layer (*NF*), in the ganglion cell layer (*GC*), at the shallow border of the inner nuclear layer (*SIN*), and the deep border of the inner nuclear layer (*DIN*) are shown. No well-focused plane exists within the inner nuclear layer (*IN*). A *white dot* near the top, left, or bottom border of four of the frames indicates a feature that is identified in Figure 5 (inset SN2) by a similar black dot on a color-coded continuity diagram of this region.

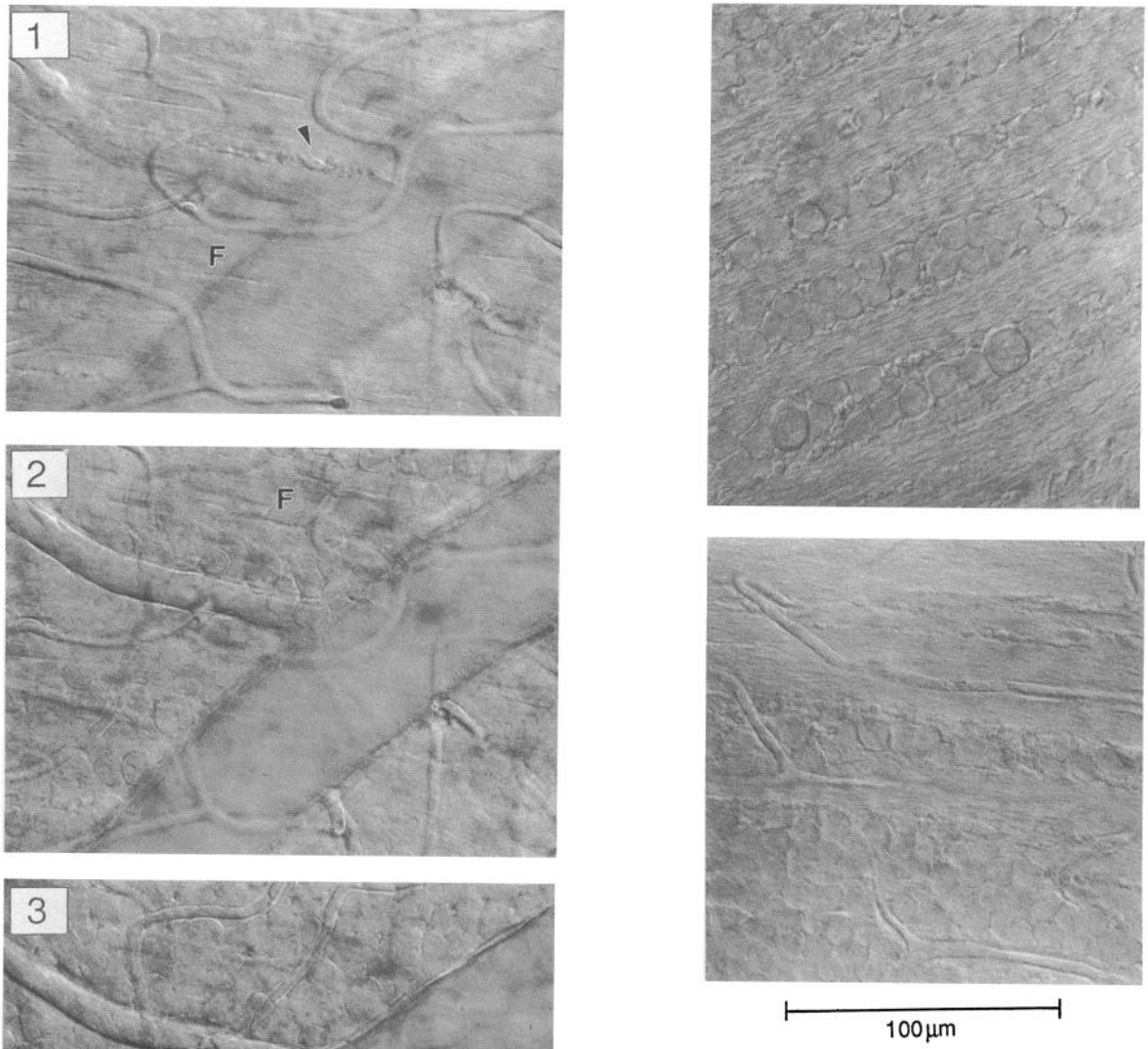

Figure 3. Neural–vascular relationships in the ganglion cell and nerve fiber layers photographed in whole-mount (DIC optics) at locations indicated in Figure 1. *Left column.* A large vein in F46R about 2.5 mm superonasal to the foveal center at location PH in Figure 1. Four focal planes at successively deeper locations show the following retinal features: (*1*) fiber bundles (*F*), a glial septum (*arrowhead*), and the nerve fiber plane of capillaries just above the ganglion cell layer; (*2*) the top (vitread) surface of the vein, 11 μm lower, where some fiber bundles are still visible, interspersed with rows of ganglion cells; (*3*) the widest part of the vein, another 12 μm lower, with the vessel wall in best focus surrounded by cell bodies; and (*4*) the bottom (sclerad) surface of the vein, another 35 μm lower, receiving a tributary vessel from the sclerad capillary network (*arrowhead*). *Right column*: *Top,* Interdigitating rows of cell bodies and fiber bundles in F22R at the boundary between the ganglion cell layer and the nerve fiber layer at inferotemporal location PH in Figure 1. *Bottom,* Capillaries in the nerve fiber/ganglion cell boundary region of F22R at location SN1 in Figure 1.

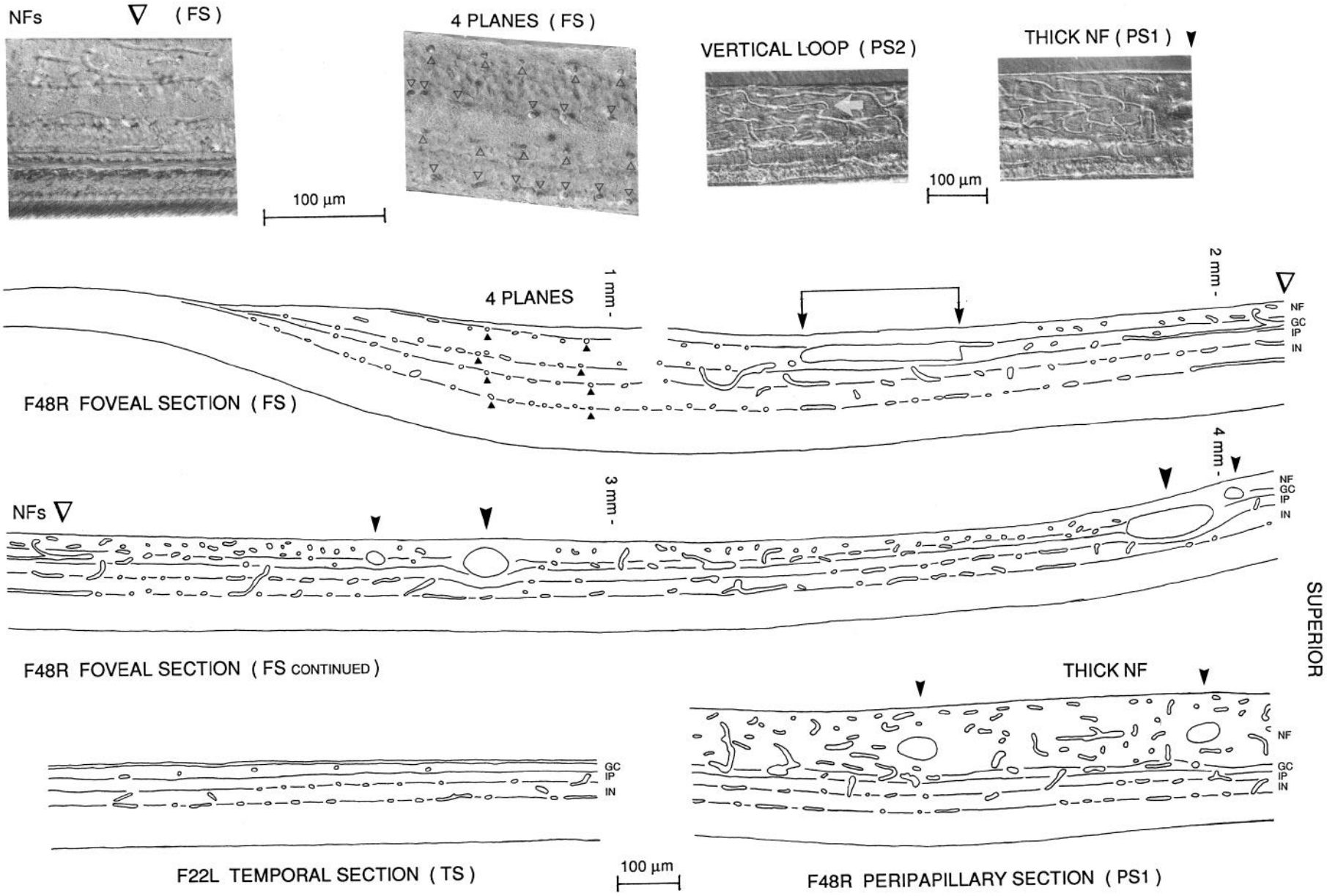
NFs
(FS)
100 µm
4 PLANES (FS)
VERTICAL LOOP (PS2)
100 µm
THICK NF (PS1)
4 PLANES
1 mm
2 mm
NF
GC
IP
IN
F48R FOVEAL SECTION (FS)
3 mm
4 mm
NFs
NF
GC
IP
IN
SUPERIOR
F48R FOVEAL SECTION (FS CONTINUED)
THICK NF
NF
GC
IP
IN
GC
IP
IN
F22L TEMPORAL SECTION (TS)
100 µm
F48R PERIPAPILLARY SECTION (PS1)

An avascular zone at the center of the fovea is surrounded by capillary networks interconnecting an approximately radial array of alternating arteries and veins. We have only seen one example of a macaque retina lacking a clear foveal avascular zone; it will be described in a subsequent publication.

As expected, a zone of reduced capillary density is apparent around the arteries. An experienced observer can detect this immediately because it results in few capillaries crossing above the arteries. Since the arteries are in the ganglion cell layer, they are far enough above the sclerad capillary network to have less impact on it, and many capillaries can be seen to cross underneath the arteries.

The side branches of the arteries often exit abruptly, nearly orthogonal to the main trunk (Wise et al., 1971). The horizontal side branches send secondary vertical branches up and down to feed the vitread and sclerad capillary networks as previously illustrated (Snodderly and Weinhaus, 1990). However, among the terminal arterial branches, this pattern is modified and the angles assumed by the branches become less abrupt and more dichotomous. This is particularly apparent in Figure 5 for A6 and for the long inferior branch of A2.

The venous tributaries have a quite different distribution and geometry. On the venous side of the circulation, vessels in each of the capillary planes usually converge onto tributaries that then drain into the main venous trunk. A particularly large tributary in the deep inner nuclear plane drains into the main trunk in the ganglion cell layer, often near the foveal crest, at around 750–850 μm eccentricity (V1, V3, V4, V6). Near the horizontal meridian, this convergence point can be closer to the center of the fovea (V5) or farther away (V2).

At the convergence between the tributary in the deep inner nuclear plane and the main trunk in the ganglion cell plane, the shallow inner nuclear plane usually drains into the main venous trunk as well. This is a departure from the pattern in the squirrel monkey, where the shallow inner nuclear plane usually drains into smaller vessels in the ganglion cell plane instead of directly into the main trunk (Snodderly and Weinhaus, 1990).

The nerve fiber capillary plane can drain into the main venous trunk at about the same point as the other capillary planes, creating a quadriconvergence of all capillary planes (V1, V6), or more commonly, it can drain into the main trunk more eccentrically. When this occurs, there can be a triconvergence of the deep inner nuclear, shallow inner nuclear, and ganglion cell planes onto the main trunk at one eccentricity followed by drainage of the nerve fiber capillary plane into the main trunk at a slightly greater eccentricity (V2, V3, V4).

As previously noted (Shimizu and Ujiie, 1978), there are also many instances of individual capillaries draining directly into the main venous trunk from the different capillary planes. This contrasts with the situation on the arterial side of the circulation, where a junction between the main vessel trunk and an individual capillary is rare.

Extrafoveal regions

For the three extrafoveal regions, the drawings in Figure 5 are too small to include the major vessels so that the connections to them are not shown. Region T is from the temporal retina near the raphe (Fig. 1) where the nerve fiber layer was only 9 μm thick; the nerve fiber capillaries were absent except for one capillary segment in the lower right. Region SN2, from the superonasal retina where the nerve fiber layer was 57 μm thick, had two layers of nerve fiber capillaries. Region P4, from the peripapillary retina where the nerve fiber layer was 110 μm thick, had a dense nerve fiber capillary plexus that was multilayered.

Note that in the drawings of all retinal regions the capillary segments have a relatively uniform diameter. This contrasts with the situation in skeletal muscle, where the capillaries are tapered; their diameter increases as they pass from the arterial to the venous side of the circulation (Caro et al., 1978; Wiedeman, 1984). The taper may be related to the greater length of capillary segments in muscle (500–1000 μm) compared to those in retina.

Orientation of nerve fiber capillaries

In all regions of the retina, the long segments of the nerve fiber capillary plexus were predominantly oriented parallel to the nerve fibers coursing toward the optic disk. This is evident in all the drawings of Figure 5. Because of our criteria for assignment to this capillary grouping, however, there are exceptions to this rule when the capillaries are not immediately surrounded by nerve fiber bundles.

To illustrate the nerve fiber capillary grouping of the foveal region more clearly, it has been abstracted in Figure 6. The trajectories of the nerve fiber bundles were drawn separately and then superimposed on the vascular network as a series of

←

Figure 4. Neural–vascular relationships seen in vertically oriented sections perpendicular to the retinal surface. See Figure 1 for section locations in F48R and F22L. Superior is to the right for all sections. *Photographs of local regions (DIC optics),* The *top row* shows photos of selected regions of the sections drawn in the *lower rows,* in addition to one section not drawn. The depth of field of the photographs is greater and the focal planes are slightly different from those of the drawings, so some details in the photos are not present in the drawings. *Drawings,* The outermost boundaries drawn for the sections are the vitreous surface and the inner segment/outer segment junction of the photoreceptors. The inner retinal layers are indicated as follows: *NF,* nerve fiber layer; *GC,* ganglion cell layer; *IP,* inner plexiform layer; *IN,* inner nuclear layer. The foveal section (*FS*) from F48R requires two rows because of its length. *Row 2* is its central segment and *row 3* is its more eccentric continuation. Retinal eccentricity is marked above the drawing at 1 mm intervals. Just beyond 2 mm eccentricity in *row 2,* the drawing is interrupted at the *inverted open triangle*; after a small region of overlap indicated by the repeat of the triangle, the section continues in *row 3. Arrowheads* point to major vessel intersections similarly indicated in Figure 1. Row 4 illustrates a temporal section (*TS*) from F22L (*bottom left*) and a peripapillary section (*PS1*) from F48R (*bottom right*). *Relationships between photos and drawings,* The *leftmost two photographic frames* in *row 1* are from the foveal section (*FS*) in *rows 2* and *3.* To illustrate the laminar relationships clearly, the photographs are at twice the magnification of the other panels of the figure. The first frame (*NFs*), taken at the location indicated by the *large inverted open triangle* just beyond 2 mm eccentricity, illustrates the region where the nerve fiber capillary network increases to more than a single layer (see Fig. 5 for illustrations of this from the whole-mount view). The second frame (*4 PLANES*) illustrates the region just before 1 mm eccentricity where the capillary planes tightly bracket the nuclear layers. *Small open triangles* on the photo point to capillaries cut in cross section. *Solid triangles* in the *drawing* immediately beneath the photo in *row 2* point to the leftmost and rightmost capillary in each plane. The third and fourth photos are from peripapillary regions *PS2* and *PS1* in F48R (Fig. 1). The third photo (*PS2*) illustrates a vertical loop (*large white arrow*) in the nerve fiber layer (region not drawn). The fourth frame (*THICK NF*) illustrates a multilayered capillary network within the nerve fiber layer. It is drawn in the *lower right corner* of the page (*F48R PERIPAPILLARY SECTION, PS1*). The *arrowhead* at the *upper right corner* of the photo corresponds to the *rightmost arrowhead* above the drawing.

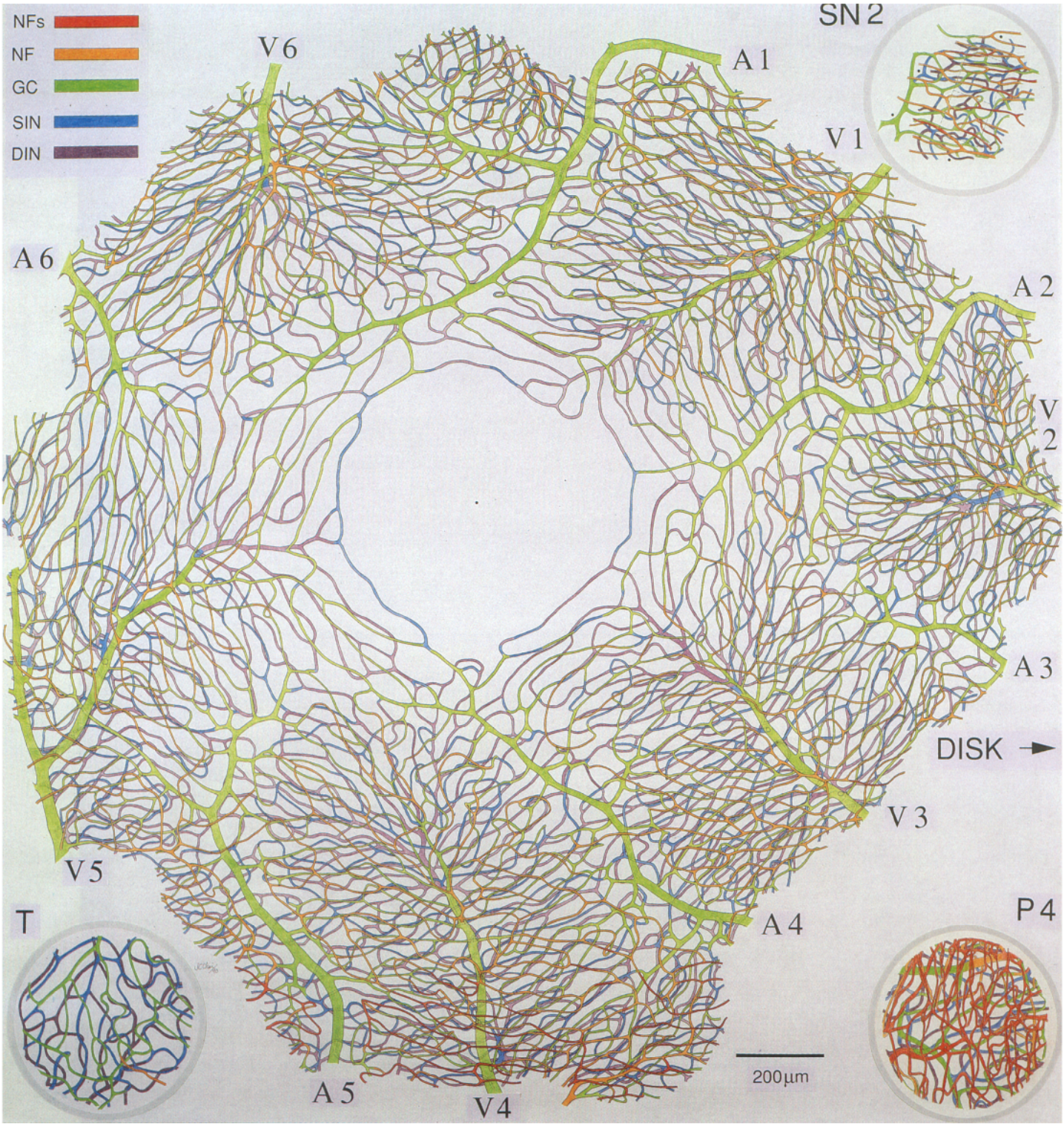

Figure 5. Depth-coded continuity diagrams of the entire retinal vasculature of four retinal regions: the fovea (*center*), a temporal region (*T*), and a superonasal region (*SN2*) of F22R, and a peripapillary region (*P4*) of F22L, all drawn to the same scale and correctly oriented. A *black dot* marks the center of the fovea, and arteries *A1–A6* and veins *V1–V6* are individually identified for reference. The retinal areas of which the drawings were done are enclosed in dotted lines in Figure 1. Photos at different depth planes from region SN2 are shown in Figure 2. Each white dot on the photos of Figure 2 identifies a distinctive feature of each capillary plane that is marked by a corresponding *black dot* in the drawing of *SN2*. The two squares formed by the *dashed lines* in *SN2* (visible with a magnifier) are the sampling areas used for quantitative measures of the capillary network. Abbreviations for the capillary groupings in the color key are the same as in Figure 2 except for the addition of *NFs*, the more superficial capillaries in the nerve fiber layer. Where an overlying vessel occludes parts of the network, the paths of the vessels crossing underneath are outlined by broken dark lines. Vertical interconnections are indicated by open circles drawn inside the tubular vessels. The original drawing of the foveal network is 1 m × 1 m and is a composite derived from more than 80 microscope fields.

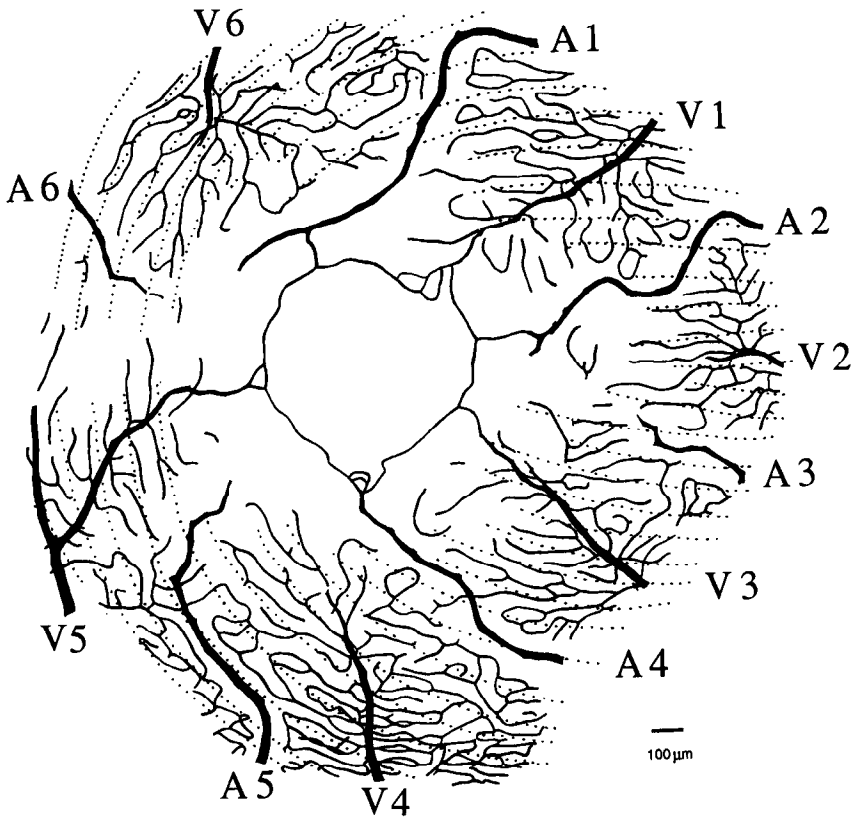

Figure 6. Capillaries in the nerve fiber layer (*NF* and *NFs*) and major arteries and veins of F22R abstracted from the complete continuity diagram of Figure 5. *Dotted lines* show the orientation of the nerve fiber bundles coursing toward the disk.

dotted lines. This comparison confirms that in most of the foveal region the long segments of capillaries assigned to the nerve fiber grouping are parallel to the path of the nerve fibers. A region exhibiting exceptions to this rule is evident between V1 and A2, however. Less extensive exceptions can also be seen between V6 and A1 and V5 and A5. The capillaries not parallel to the nerve fibers are generally either in the ganglion cell layer above (superficial to) the main ganglion cell plane, or at the border between the ganglion cell layer and the nerve fiber layer, as illustrated in Figure 3.

Quantitative measures of the capillary network

Although it is generally expected that the capillary volume of the retina should increase with retinal thickness (Michaelson, 1954; Chase, 1982), the diagrams of Figure 5 imply that variations in the thickness of the nerve fiber layer could play an unexpectedly large role. To investigate this, we calculated for each sampling area the capillary volume in each of the capillary groupings, as well as the total capillary volume of the retina. The results for four retinal sectors are plotted in Figures 7–10. Although the sampling locations depart from strict linear geometry, for simplicity of presentation we have plotted the data along a single eccentricity axis as a schematic profile.

Data from the fovea, a peripapillary region, and a temporal region near the horizontal raphe have been juxtaposed to facilitate comparisons among retinal loci with widely differing characteristics. The peripapillary regions were chosen to match their total retinal thickness as closely as possible to the total retinal thickness near the foveal crest. In this way we compared vascularity of retinal regions with the same total thickness but very different thicknesses of individual layers.

Total capillary volume of the retina

Figure 7 summarizes the effects of retinal location on total capillary volume of the retina. For F22, R and L (top row), we compare samples from the superonasal sector of the retina (right), where the thickness of the nerve fiber layer increases steeply with eccentricity, with samples from the superotemporal sector (left) where the nerve fiber layer is less prominent. For F46R and F54R (bottom row), the majority of the samples were distributed vertically.

In all cases, the capillary volume increases steadily with eccentricity from the terminal capillary ring surrounding the foveal avascular zone to the foveal crest, near 1 mm eccentricity. In retinal sectors where the nerve fiber layer does not reach its maximum thickness (superotemporal, superior, and inferior), the capillary volume changes relatively little from about 1 to 3 mm eccentricity (Fig. 7, upper left, lower left, lower right). Where the nerve fiber layer is thickest, in the superonasal sector (upper right) and in the peripapillary regions (all panels), the capillary volume is greatest. This is true in spite of the fact that the total retinal thickness of the peripapillary regions is comparable to the total thickness of the retina at the foveal crest. The capillary volume is least in the temporal loci where both the nerve fiber layer and the total retina are relatively thin.

These data show that in the extrafoveal retina, the volume of capillaries is not a simple function of eccentricity. The samples in the superior, peripapillary, and temporal regions of F46R and those from the inferior, peripapillary, and temporal regions of F54R were all within 10% of the same eccentricity. The key factors appear to be the thickness and composition of individual layers of the inner retina.

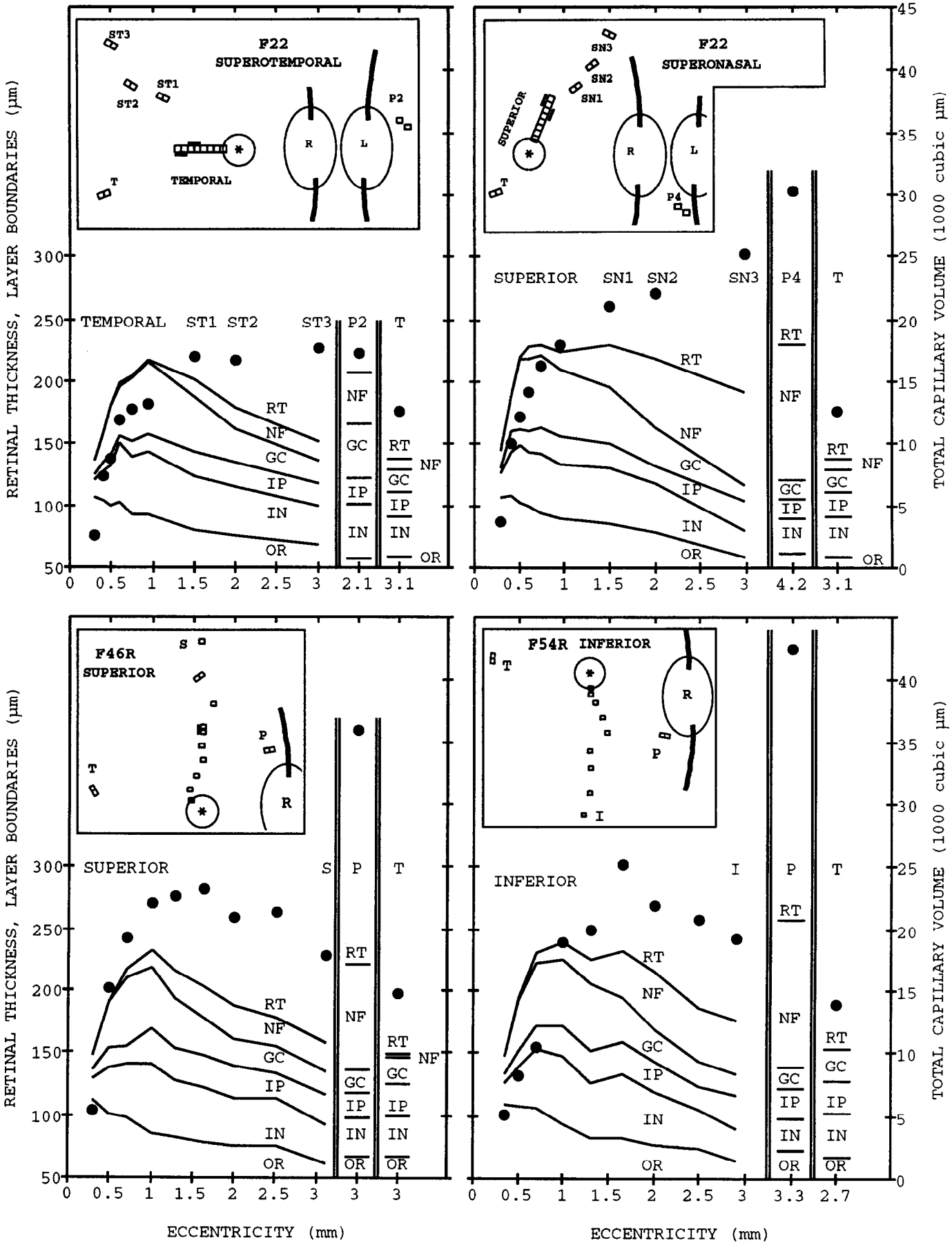
F22
SUPEROTEMPORAL
ST3
ST1
ST2
P2
TEMPORAL
T
R
L
TEMPORAL ST1 ST2 ST3 P2 T
RT
NF
GC
IP
IN
OR
0 0.5 1 1.5 2 2.5 3 2.1 3.1
F22
SUPERONASAL
SN3
SN2
SN1
SUPERIOR
P4
T
SUPERIOR SN1 SN2 SN3 P4 T
0 0.5 1 1.5 2 2.5 3 4.2 3.1
F46R
SUPERIOR
S
P
T
SUPERIOR S P T
0 0.5 1 1.5 2 2.5 3 3 3
F54R INFERIOR
I
INFERIOR I P T
0 0.5 1 1.5 2 2.5 3 3.3 2.7
RETINAL THICKNESS, LAYER BOUNDARIES (µm)
TOTAL CAPILLARY VOLUME (1000 cubic µm)
ECCENTRICITY (mm)
ECCENTRICITY (mm)

Volumes of the separate capillary groupings

The volumes of the four capillary groupings associated with individual retinal layers are illustrated in Figure 8. These data are drawn from the same sampling regions as Figure 7 and are plotted in the same format to facilitate comparisons with neuronal layer thicknesses.

The volume of the nerve fiber capillary plexus closely follows variations in thickness of the nerve fiber layer. It is low in the temporal retina where the nerve fiber layer is thin, and it increases in the nasal retina, being greatest in the peripapillary region where the nerve fiber layer is thickest. Within the fovea, the nerve fiber grouping is less voluminous than the other capillary planes and it increases more slowly in volume with retinal eccentricity. It does not become more voluminous than the neighboring ganglion cell plane until well outside the foveal depression. Sampling variability precludes any precise comparisons of the two components of the vitread network in the parafoveal regions.

In the sclerad capillary network, the deep inner nuclear plane is usually more voluminous than the neighboring shallow inner nuclear plane. The volume of the deep inner nuclear capillary plane increases rapidly with eccentricity in the fovea and then remains at a relatively constant level throughout the central retina. It is interesting to note that the cone pedicles, which are just sclerad to these capillaries, reach their maximum density at about the same eccentricity where the volume of this capillary plane has climbed to its plateau (Schein, 1988).

The shallow inner nuclear plane shows individual variation from one animal to another. It is less voluminous than the deep inner nuclear plane in all retinal sectors of F22, including the nasal and inferior sectors not illustrated. For F46, many sampling regions have comparable values for the two planes. F54 shows a mixed picture, with the shallow inner nuclear plane less voluminous in most samples but about equal to the deep plane in others.

Volumes of the vitread and sclerad capillary networks

To reduce the variability shown by the individual capillary groupings, we pooled the data as a sclerad network bracketing the inner nuclear layer and a vitread network associated with the ganglion cell and nerve fiber layers (Fig. 9). We felt that merging the ganglion cell and nerve fiber capillaries was functionally justified because of the frequent intermingling of ganglion cells and nerve fibers, as discussed earlier. Furthermore, combining the two planes bracketing the inner nuclear layer did not obscure any of the points we wished to emphasize. In fact, the sampling variability diminished, the differences among animals were minor, and we were able to analyze the effects of the thickness of retinal subdivisions. The patterns that emerged are as follows.

Within the fovea, the sclerad network is more voluminous; the volumes of both networks increase rapidly with eccentricity. Outside the fovea, the volume of the sclerad network is similar from one animal to another and varies little with retinal location. In contrast, the vitread network varies drastically with retinal location, increasing where the retina and the nerve fiber layer are thick, and decreasing where they are thin. As a result, the sclerad network is the more voluminous one in the temporal retina and the vitread network dominates in the peripapillary region and the superonasal region. The two networks have similar volumes near the vertical meridian where nerve fiber layer and total retinal thickness are intermediate (represented by the samples from F46 and F54).

Percentage of the tissue volume occupied by capillary lumens

The question that arose from this analysis was what caused the topographic variations in the volume of the vitread network. We considered two main possibilities. First, differences in the thickness of the outer retina create variations in the path length for diffusion of oxygen (and perhaps other nutrients) from the choroid. However, the pattern of topographic variations is not consistent with this view (see below). The more likely possibility is that the topographic variations in capillary volume are linked to local variations in demand for oxygen and other metabolites.

We particularly wanted to know whether there might be a higher *density* of capillaries in the vitread network, which would cause variations in nerve fiber and ganglion cell layer thickness to contribute disproportionately to the topographic variations in the vasculature. To evaluate this possibility, we calculated for each sampling area the percentage of the tissue volume occupied by capillary lumens (called percent capillary volume) for two retinal subdivisions and for the total retina. The percent capillary volume of the tissue supplied by the vitread network was calculated using the volume of the retina between the vitreous surface and the deep border of the ganglion cell layer. The percent capillary volume of the inner retina was calculated using the volume of the retina between the vitreous surface and the deep border of the inner nuclear layer. For comparison, the percent capillary volume of the total retina was calculated using the volume of the retina between the vitreous surface and the vitread border of the retinal pigment epithelium. The results are summarized in Figure 10, using the same format as Figures 7 and 9.

The percent capillary volume of the total retina is lowest in the fovea and highest in the peripapillary region. The values for region P2 of F22L are not as high as the other peripapillary

←

Figure 7. Total retinal thickness (*RT*), neuronal layer boundaries, and total capillary volume as a function of retinal location. In each panel, schematic drawings (not to scale) abstracted from Figure 1 identify the sampling areas from which the data were derived. The center of the fovea is indicated by an *asterisk* in a *circle* that represents the foveal avascular zone. For each panel, the *left vertical axis* gives the scale for the thickness of the retina and the distance of the layer boundaries from the retinal pigment epithelium, indicated by *curves* formed by *solid lines*. The outer retina (*OR*), comprised of the photoreceptors and the outer plexiform layer, and the individual layers of the inner retina are labeled (see Fig. 4 for abbrevations). The *right vertical axis* is the scale for total capillary volume of the retina, indicated by the *solid circles*. The *horizontal axis* indicates eccentricity from the foveal center; the axis is segmented by *double vertical lines* after 3.2 mm so that peripapillary and temporal loci can be juxtaposed to the other regions. For *F22* the retinal thickness of a peripapillary region was matched within 5% with the retinal thickness at the foveal crest, by pairing peripapillary regions from the left eye with foveal regions from the right eye. For the other two animals, the worst mismatch occurred for *F54R*, where the retinal thickness in the peripapillary region was about 10% greater than at the foveal crest. Because of lack of space in the representations of the peripapillary regions *P2* and *P4* in the *upper panels*, labels are omitted for *RT* and *OR* in the *upper left panel*, and for *OR* in the *upper right panel*. The nerve fiber layer was not visible in the temporal region represented in the *lower right panel*.

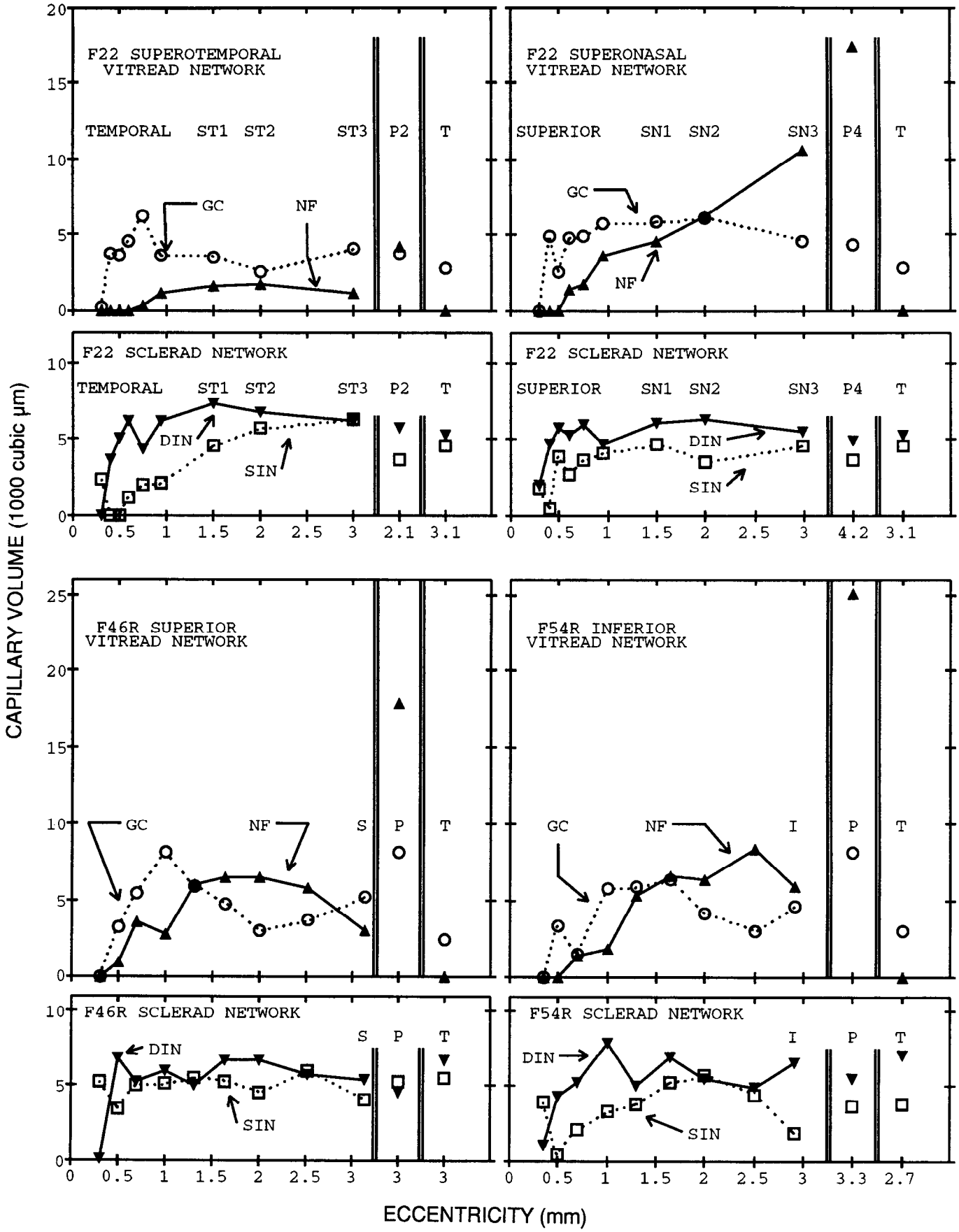

Figure 8. Volumes of the individual capillary planes or groupings in the same retinal regions used for Figure 7. There are two panels for each retinal sector; the *upper panel* displays data for the nerve fiber grouping (*NF, solid triangles*) and ganglion cell plane (*GC, circles*), which form the vitread network. The *lower panel* for each sector displays the volumes of the shallow inner nuclear (*SIN, squares*) and deep inner nuclear planes (*DIN, inverted solid triangles*), which form the sclerad capillary network. All panels have the same vertical scale.

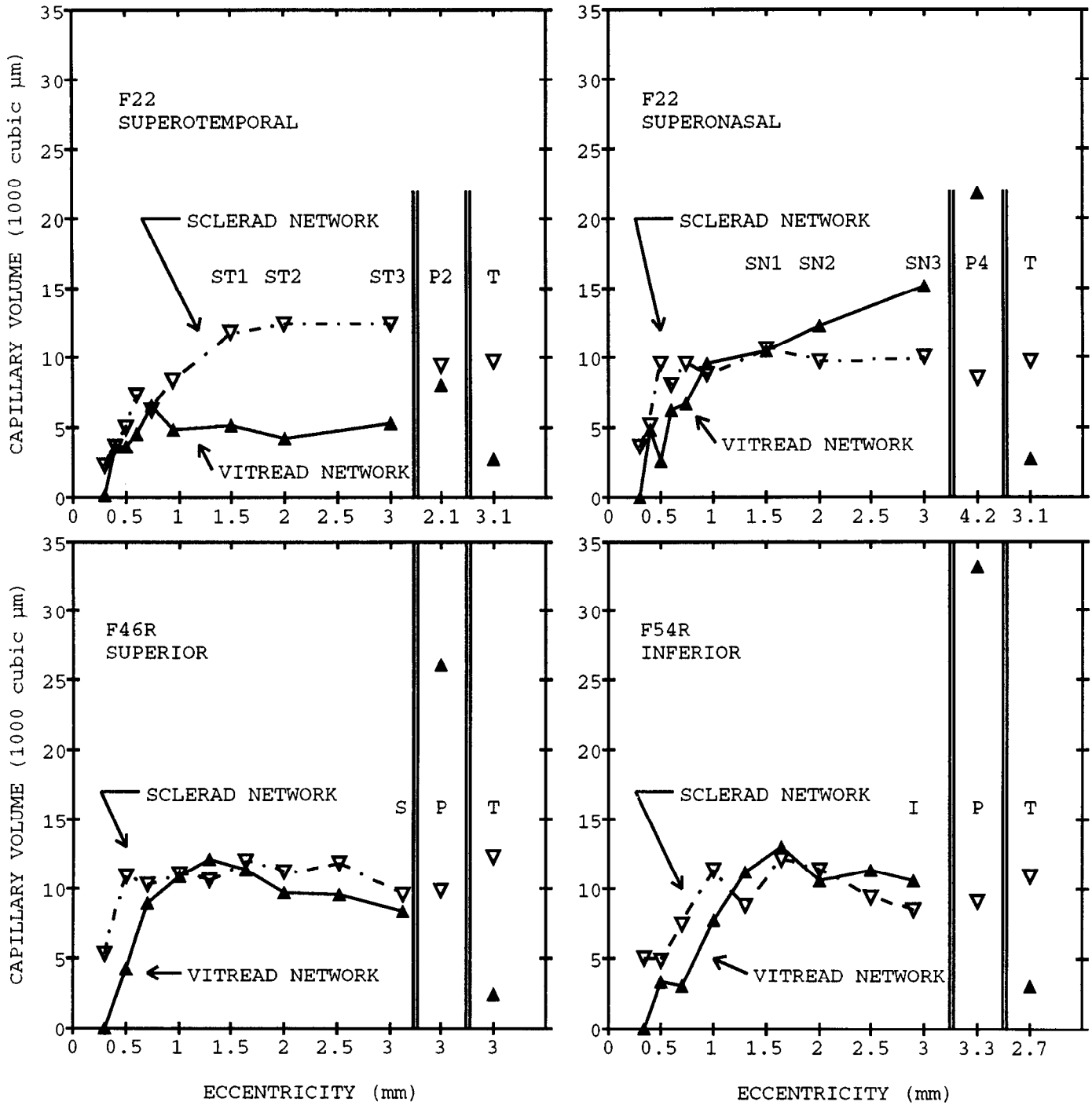

Figure 9. Capillary volumes of the vitread and sclerad networks in the same retinal regions used for Figures 7 and 8. *Inverted open triangles,* sclerad network; *solid triangles,* vitread network.

points because it was farther from the disk and the nerve fiber layer was relatively thin. Percent capillary volumes of the total retina in the peripapillary sampling areas not plotted (P of F22R; P1 and P3 of F22L) were 1.6–1.7%. This shows that the peripapillary region is the most densely vascularized part of the retina, whether measured as total volume of capillaries or as the percentage of tissue volume occupied by capillaries. It implies that the nerve fiber layer, which is maximally thick in the peripapillary region, has an especially strong influence on retinal vascularity.

The converse situation, namely, what happens in retinal regions where the nerve fiber layer is thin, is illustrated by comparing the percent capillary volume for the vitread network with that of the whole inner retina. For reference, we note that in the nasal perifovea and the peripapillary regions where the nerve fiber layer is thick, the vitread network and the whole inner retina have similar capillary densities. However, within the fovea and in the temporal retina where the nerve fiber layer is thin, the vitread network has a lower capillary density than the inner retina as a whole. Thus, where the nerve fiber layer is thin,

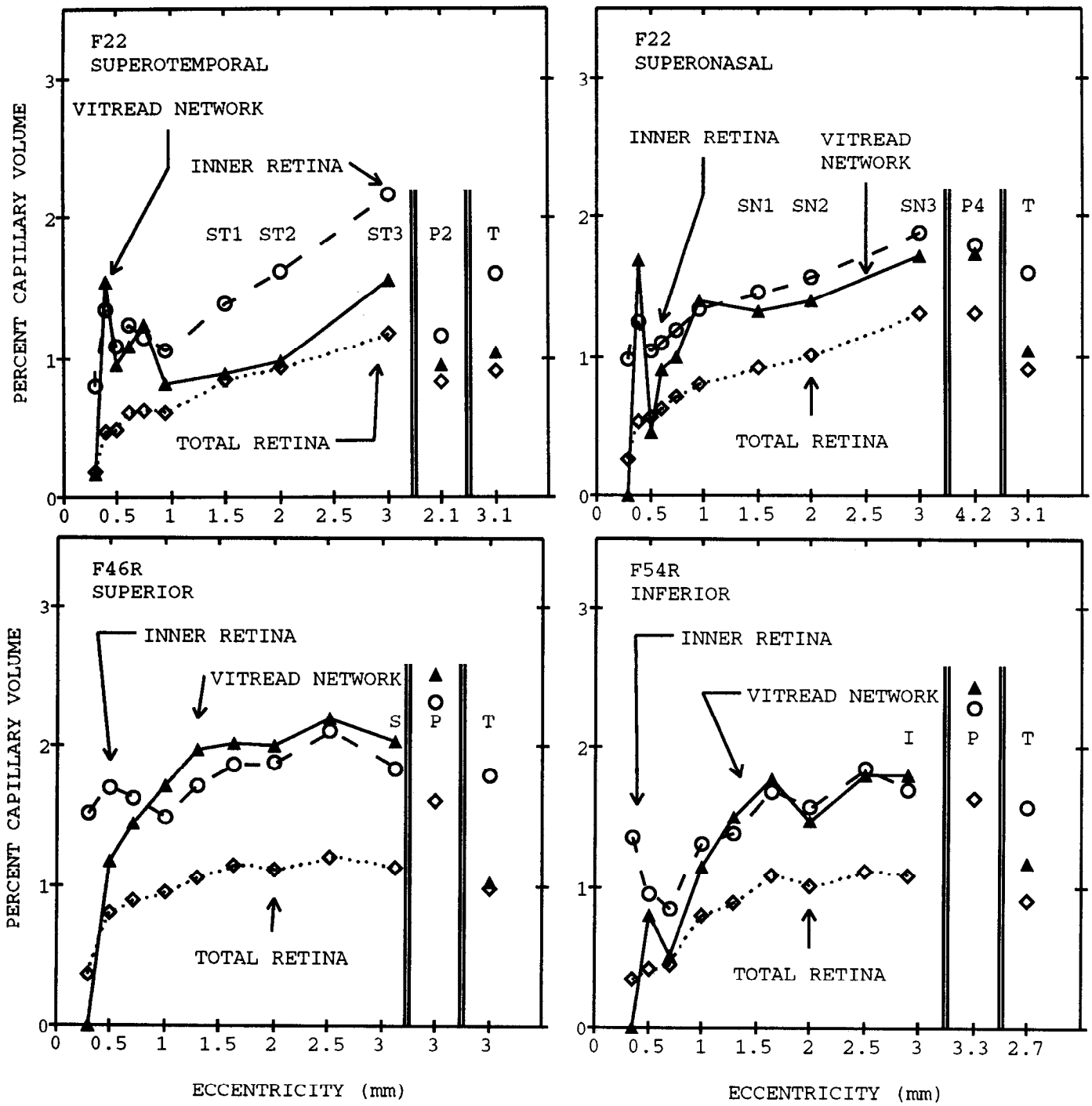

Figure 10. Percentage of tissue volume occupied by the capillary lumens of the vitread network, the inner retina, and the total retina for the same retinal regions used for Figures 7–9. The inner retina extends from the vitreous surface to the deep border of the inner nuclear layer. The total retina extends from the vitreous surface to the vitread border of the retinal pigment epithelium. *Circles,* inner retina; *solid triangles,* vitread network; *diamonds,* total retina.

the capillary *density* of the vitread network (Fig. 10), as well as its *volume* (Fig. 9), is reduced. We interpret this as additional evidence that the nerve fiber layer profoundly influences retinal vascularity.

Relationships between the thickness of retinal subdivisions and their vascularity

The capillary volume of the retina increases monotonically as the thickness of the retina increases in the fovea (Fig. 7), but the relationships between vascularity and the thickness of the retina and its subdivisions are more complicated in the extrafoveal regions. To examine these relationships, we combined the data into two sets, one from F22 and the other from F46 and F54.

First, we asked whether the thickness of the avascular outer retina interposed between the choroid and the retinal capillary network has a systematic influence. A positive answer to this question would imply that diffusion of oxygen or other metab-

olites from the choroid, with its high blood flow rate and high oxygen tension (Bill, 1984), could be a factor shaping the retinal capillary network.

If diffusion distance from the choroid were a major influence, we should expect to see retinal vascularity increase along with increasing retinal thickness. This does happen, but when the relationship is plotted (Fig. 11, top row), locations in the fovea form a separate group from locations outside it. Furthermore, the data are widely dispersed. These features of the graphs suggest that the *maximum* diffusion distance from the choroid is not uniformly effective in determining retinal vascularity.

The importance of diffusion distance from the choroid was examined further by plotting the total capillary volume as a function of the *minimum* diffusion path from the choroid (Fig. 11, middle row). Since the outer retina from the deep border of the inner nuclear layer to the retinal pigment epithelium has no vessels, its thickness is the minimum path from the choroid to the vascularized retina. A negative relationship between the retinal capillary volume and the thickness of the outer retina was evident in the fovea, and no clear pattern could be discerned for the extrafoveal retina. This is the opposite of what would be predicted if diffusion distance from the choroid were a strong determinant of retinal vascularity.

The more attractive interpretation is that the capillary volume is primarily determined by the volumes of the retinal subdivisions with which the capillary networks are associated. This would imply that local metabolic activity is the dominant force determining the development and maintenance of the capillary network. This view is partially supported by the strong positive association between the volume of the retinal capillary network and the thickness of the inner retina, which is the vascularized portion (Fig. 11, bottom row). For F22, the correlation as determined by Spearman's rank correlation coefficient, r_S, is 0.88.

The association between capillary volume and tissue thickness was examined in more detail by plotting separately the volumes of the vitread and sclerad networks as a function of the thickness of the retinal subdivisions with which they are associated (Fig. 12). For F22, the volume of the vitread network was tightly linked to the combined thicknesses of the nerve fiber and ganglion cell layers (top row; $r_S = 0.91$). Also, in this instance the data from the foveal and extrafoveal regions intermix so that a uniformly applicable relationship seems to hold. The relationship is not linear. There is a threshold thickness near 20 μm below which only an occasional vessel is found, with no well-developed network. As the thickness increases, the capillary volume increases in a curvilinear fashion with the highest values in the peripapillary region. A similar pattern can be seen in the data from F46 and F54, but it is less clear because of individual differences between animals and the smaller number of data points. One aberrantly low point for F54 at thickness 60 μm is apparently due to sampling variability associated with the placement of our sampling area at 700 μm eccentricity.

The contrast between the vitread and the sclerad capillary network is dramatically shown by the graphs in the second row of Figure 12. The data from the extrafoveal regions show no relationship between the volume of the sclerad network associated with the inner nuclear layer and the thickness of the inner nuclear layer. This could be due to the fact that most of the capillaries in this network lie at the borders of the layer rather than in the interior. In this case, local factors influencing the establishment of the capillary network probably include influences from the adjacent plexiform layers that are not strictly linked to the thickness of the inner nuclear layer.

Finally, to clinch the lack of a relationship between the retinal circulation and the diffusion distance from the choroid, we show in the bottom row of Figure 12 the volume of the sclerad network as a function of the thickness of the outer retina. We reasoned that the sclerad network, being closest to the choroid, should be the network most affected by variations in the length of the diffusion path. Clearly the data do not support the importance of diffusion from the choroid. In the extrafoveal retina, there is no relationship between the thickness of the outer retina and the volume of the sclerad network, and in the fovea there is a negative relationship.

We conclude that the increase in capillary volume with increased thickness of the extrafoveal retina, particularly in the peripapillary region, mainly reflects increases in the vitread capillary network linked to thickening of the nerve fiber layer. Within the fovea, additional factors may be operating. In either case, increased retinal vascularity appears not to be caused by increases in diffusion distance from the oxygen-rich choroid.

The retinal area covered by capillaries: visual screening

Since light must traverse the retina before reaching the photoreceptors, we see the world through the screen of the retinal vascular network (Snodderly and Weinhaus, 1990). The percentage of the retinal area occupied by the capillary network is summarized in Figure 13 (top). These data show the probability that a photon will encounter one or more capillaries before reaching a photoreceptor.

As we have shown previously for the squirrel monkey (Snodderly and Weinhaus, 1990), the percent retinal area occupied by capillaries in the fovea rises sharply with eccentricity to a plateau around 40%. In the perifovea along the vertical meridian the values are mostly above 45% for two of the animals, with F22 slightly lower. The highest values, in the range of 60–70%, are in the peripapillary region. Photoreceptors in the temporal retina are screened less by capillaries.

In general, the profile of visual screening by the capillary network follows the profile of capillary volume (cf. Fig. 7). To assess the precision of this relationship, we plotted the percent retinal area covered by capillaries as a function of the total capillary volume at the same location (Fig. 13, bottom). The percent retinal area covered is proportional to the capillary volume except in the peripapillary region. There the network becomes so dense that the overlaps among capillaries cause deviation from the linear relationship. The proportional relationship between capillary volume and capillary screening in other parts of the retina may imply a developmental spacing mechanism such that capillaries growing in adjacent planes avoid each other and minimize overlap.

Capillary diameters

For predicting the flow of blood through the different neuronal layers, it is important to know the capillary diameters as well as their total volume. Histograms for all the capillary segments measured in our study are shown in Figure 14. Data from F46 and F54 were pooled, since the median capillary diameter of our total sample from F46 (5.0 μm) was not significantly different (Wilcoxon signed rank test) from the median diameter of the sample from F54 (4.9 μm).

The distributions of capillary diameters are not normal (Pearson χ^2 test of normality), but are skewed to the left with a relatively abrupt cutoff. Only two capillaries out of 1628 were

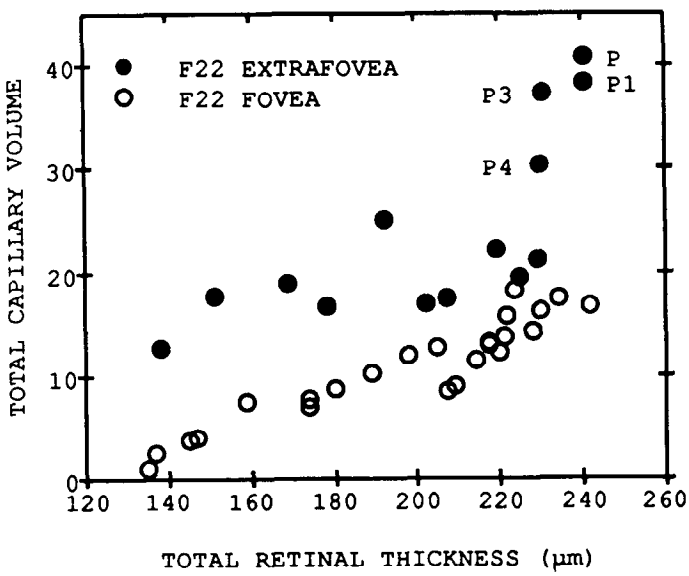
F22 EXTRAFOVEA
F22 FOVEA
P
P1
P3
P4
TOTAL CAPILLARY VOLUME
TOTAL RETINAL THICKNESS (μm)

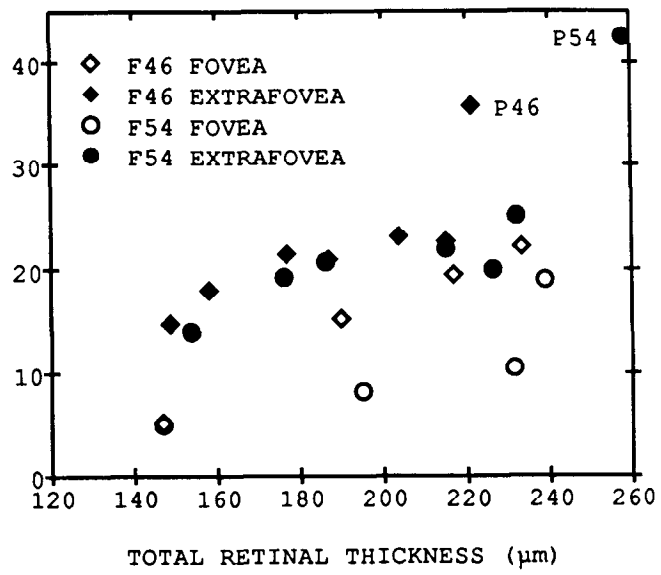
F46 FOVEA
F46 EXTRAFOVEA
F54 FOVEA
F54 EXTRAFOVEA
P54
P46
TOTAL RETINAL THICKNESS (μm)

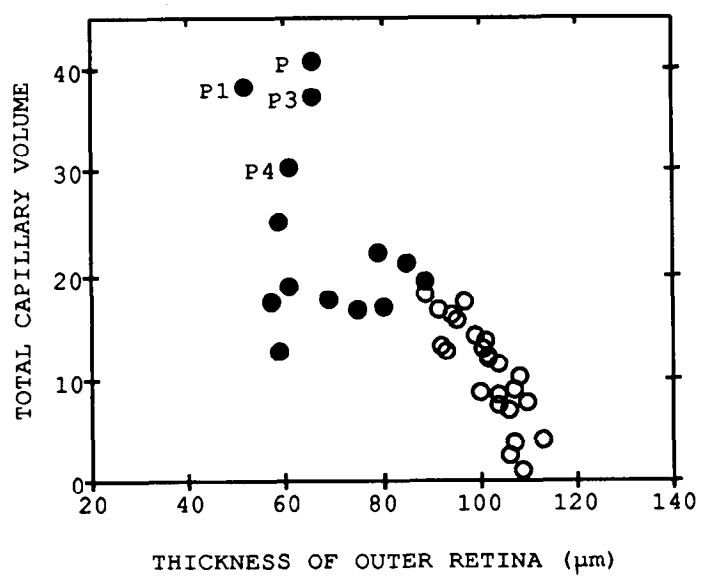
P
P1
P3
P4
TOTAL CAPILLARY VOLUME
THICKNESS OF OUTER RETINA (μm)

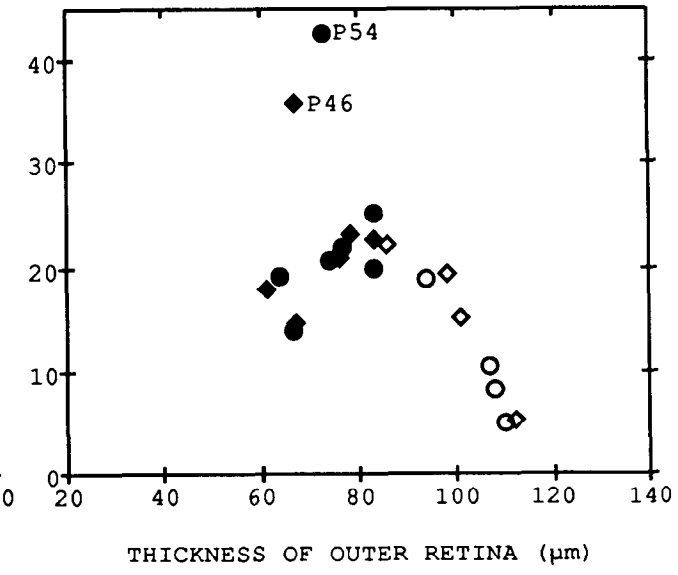
P54
P46
THICKNESS OF OUTER RETINA (μm)

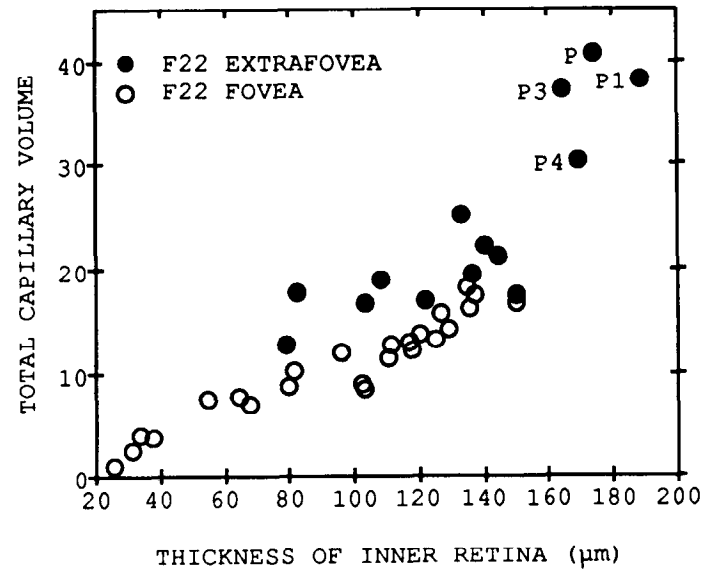
F22 EXTRAFOVEA
F22 FOVEA
P
P1
P3
P4
TOTAL CAPILLARY VOLUME
THICKNESS OF INNER RETINA (μm)

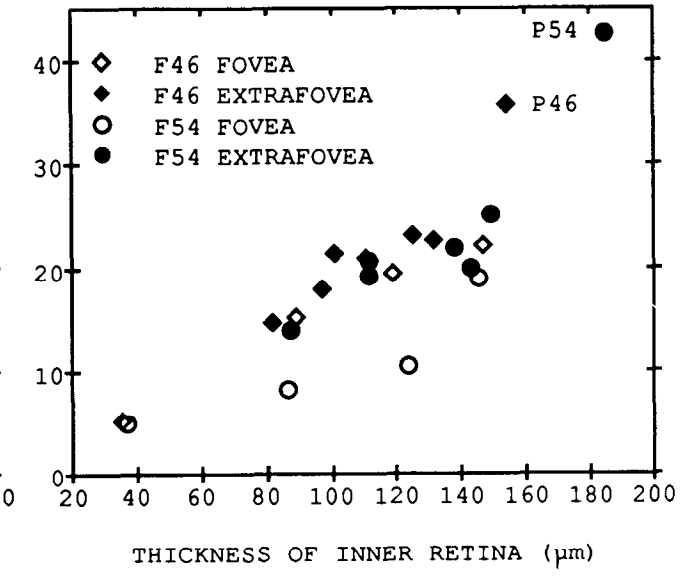
F46 FOVEA
F46 EXTRAFOVEA
F54 FOVEA
F54 EXTRAFOVEA
P54
P46
THICKNESS OF INNER RETINA (μm)

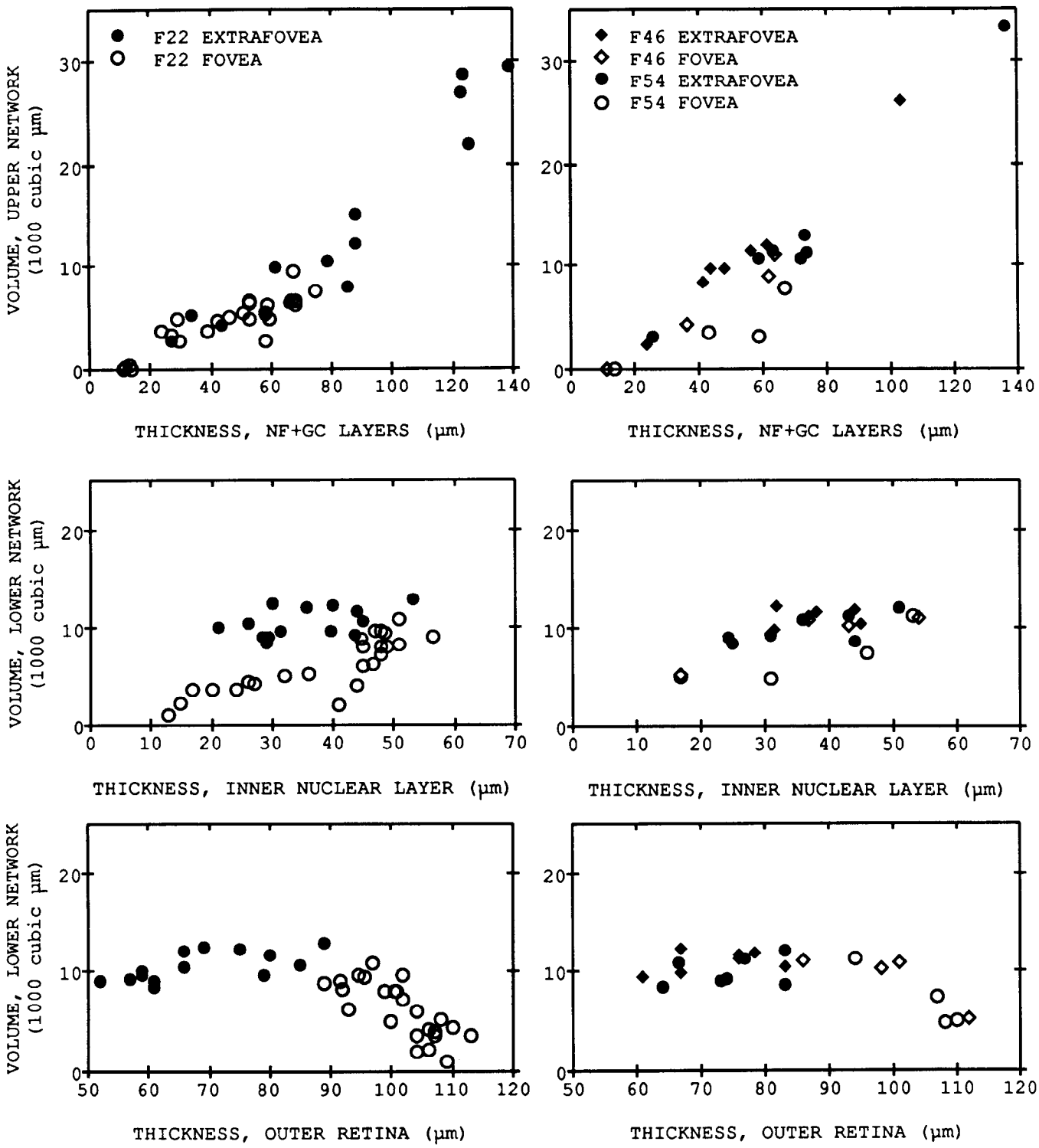

Figure 12. *Top row,* Relationship between the volume of the vitread capillary network and the combined thickness of the neural layers with which it is associated, the nerve fiber (*NF*) and ganglion cell (*GC*) layers. *Middle row,* Relationship between the volume of the sclerad capillary network and the thickness of the inner nuclear layer with which it is associated. *Bottom row,* Relationship between the volume of the sclerad capillary network and the thickness of the outer retina. *Solid symbols* indicate data from eccentricities greater than 1 mm.

←

Figure 11. Relationships between the total capillary volume of the retina and the thickness of the retina (*top row*) or the thickness of its two major subdivisions, the outer retina extending from the deep border of the inner nuclear layer to the vitread border of the retinal pigment epithelium (*middle row*) and the inner retina extending from the vitreous surface to the deep border of the inner nuclear layer (*bottom row*). Data from F22 are illustrated in the *left column,* and data from F46 and F54 are shown together in the *right column. Solid* symbols indicate data from eccentricities greater than 1 mm.

Table 1. Capillary diameters (μm)

	F22					F46 and F54 combined				
Network	Segments (*N*)	Mean	Median	Variance	Inter-quartile range	Segments (*N*)	Mean	Median	Variance	Inter-quartile range
NF	338	4.6	4.5	0.97	1.06	196	4.8	4.7	0.88	1.35
GC	256	5.0	4.8	1.08	1.25	145	4.9	4.8	1.00	1.20
SIN	200	4.9	4.9	0.44	0.91	113	5.0	5.0	0.50	0.80
DIN	237	5.2	5.0	0.65	1.00	143	5.0	5.0	0.55	1.10
Total	1031	4.9	4.8	0.87	1.12	597	4.9	4.9	0.76	1.20

NF, nerve fiber capillary network; GC, ganglion cell network; SIN, shallow inner nuclear network; DIN, deep inner nuclear network.

less than 3 μm luminal diameter; 3 μm is the smallest opening through which a human red blood cell can pass undamaged (Caro et al., 1978). Other parameters of the distributions are listed in Table 1. Because some distributions might be transformable to normal, both standard normal parameters and statistics for nonparametric analyses are provided.

The most obvious trend in the data is an increase in capillary diameter as one moves from the vitreous surface to deeper layers of the retina. The median diameter of capillaries in the nerve fiber network is significantly less than the median diameter of capillaries in the deep inner nuclear layer for both F22 ($p < 10^{-4}$) and F46 + F54 ($p < 10^{-2}$, Wilcoxon signed ranks test). Furthermore, when the data from F22 were separated into foveal, perifoveal, and peripapillary regions (not shown), the trend was maintained within each separate region.

The capillaries of the shallow inner nuclear plane are the most uniform population. The dispersion of diameters in the shallow inner nuclear plane is significantly smaller than the dispersion of diameters in both the ganglion cell plane and the nerve fiber plexus (Ansari–Bradley test) for both F22 ($p < 10^{-3}$) and F46 + F54 ($p < 10^{-2}$). This matches the visual impression one acquires during microscopy of the retina.

In the case of the nerve fiber plexus, the greater dispersion of capillary diameters is related to the large regional variations in thickness of the nerve fiber layer. The mean diameter of nerve fiber capillaries is positively correlated with both the thickness of the nerve fiber layer and with the total capillary length in the sampling area ($r_s = 0.52$–0.54, $p < 0.01$ for F22; $r_s = 0.44$–0.45, $p < 0.05$ for F46 + F54). As part of this picture, the nerve fiber capillaries in the peripapillary region tend to have larger diameters than the nerve fiber capillaries in many other retinal regions.

We thought at first that the increase in capillary diameter with increased total capillary length in the nerve fiber layer might also occur in other retinal layers as a way to increase blood flow to tissue regions that are heavily vascularized. Such a relationship could result in an underestimate of regional differences in blood flow if microvessel length were the only parameter measured (e.g., Zheng et al., 1991). However, the retinal capillary diameters, the total capillary length, and the layer thickness do not reliably increase together except in the nerve fiber layer. For example, capillary diameters in the deep inner nuclear plane are uncorrelated or negatively correlated with the total capillary lengths in the sampling areas ($r_s = -0.09$ for F22; $r_s = -0.39$, $p < 0.05$ for F46 + F54). To understand fully the functional implications of the regional differences in capillary networks, it seems likely that vascular geometry will have to be studied in conjunction with physiological measurements such as blood flow and metabolite diffusion and utilization.

Discussion

The laminar distribution of retinal capillaries

The laminar distribution of capillaries in the fovea of macaque monkeys is similar to that described previously for squirrel monkeys; comparisons with other species have been summarized in our earlier report (Snodderly and Weinhaus, 1990). The present article extends our studies to extrafoveal loci in the central retina. Outside the fovea, the topographic variations in the thickness of the nerve fiber layer become a dominant factor in the vascularity of the retina. Wherever the nerve fiber layer is thick, it contains a dense, multilayered capillary plexus.

Earlier measurements of optic disk tissue, where the neural constituents are only optic nerve fibers, showed a higher density of capillaries than the heterogeneous inner retina (Quigley et al., 1982; Wilson et al., 1988). The values obtained for the percent capillary volume of the disk (2.2–2.6%) and those we found for the vitread capillary network where the nerve fiber layer is thick (1.8–2.6%) are similar to data from gray matter of the visual cortex of the rat (2.1%; Bar, 1980) and large areas of the cerebral cortex of the cat (2.8%, Wiederhold et al., 1976; 1.8–2.5%, Pawlik et al., 1981).

The dense vascular network of the retinal nerve fiber layer implies a substantial metabolic demand. A high metabolic rate is presumably required for ion pumping because the optic nerve fibers within the eye are unmyelinated. This suggestion is consistent with the cytochrome oxidase staining patterns of the retina, which show that oxidative enzyme levels drop abruptly when the nerve fibers become myelinated behind the lamina cribrosa (Kageyama and Wong-Riley, 1984). The importance of myelination has been further corroborated by studies of the metabolism of the retrobulbar optic nerve. As the optic nerve leaves the eye and runs to the optic chiasm, its myelination first increases and then decreases. Those loci with less myelin have higher blood flow and higher glucose uptake (Sperber and Bill, 1985).

Retinal thickness and vascularity

The fact that the retinal vascular network is attenuated or absent in many animal species with thin retinas focused attention initially on the importance of diffusion of metabolites from the choroidal circulation to supply the retina (Michaelson, 1954; Chase, 1982). However, more recent work has shown that avas-

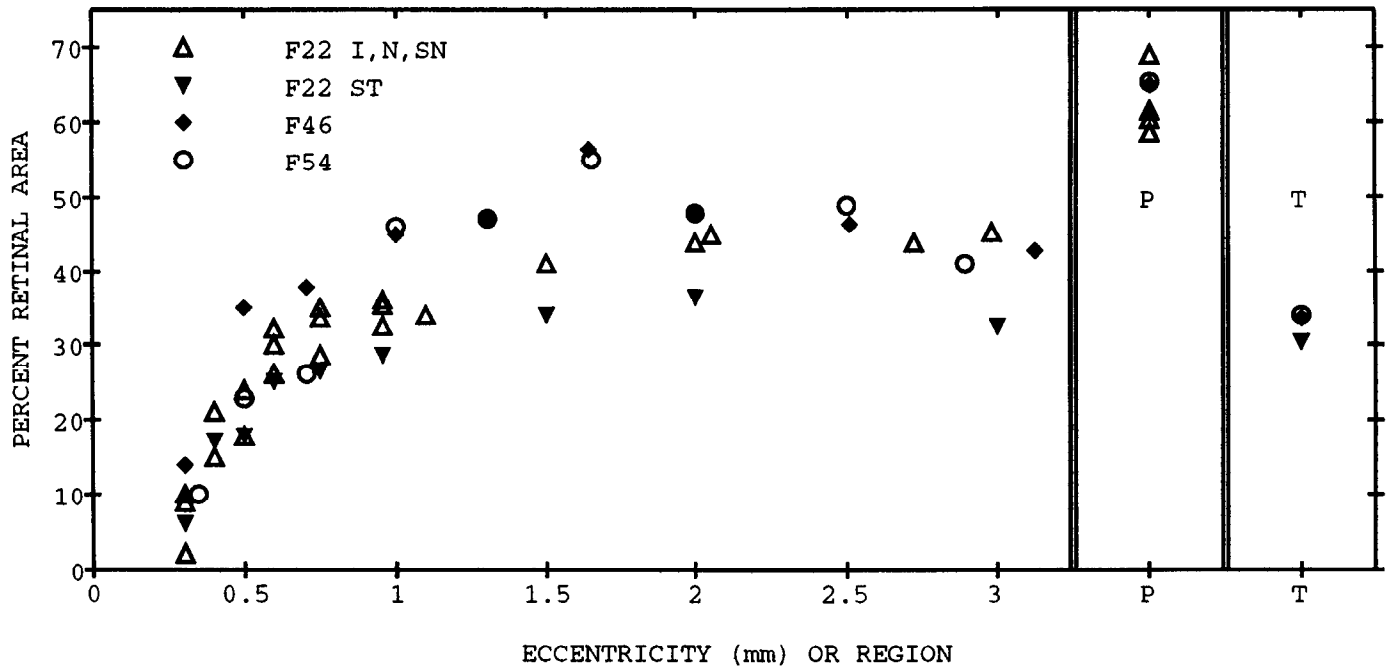

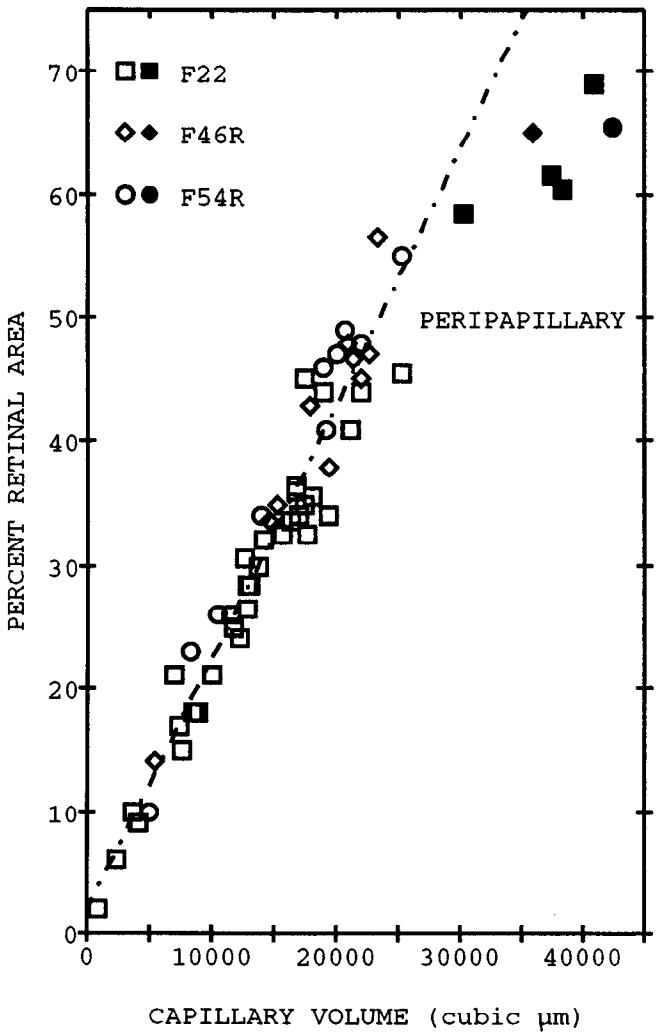

Figure 13. Percentage of the retinal area occupied by the capillary network. *Top,* Data from three animals plotted as a function of retinal eccentricity or as assigned to the peripapillary (*P*) or temporal (*T*) regions indicated in Figure 1. Data from the superotemporal sector of F22 (*ST*) are indicated with a different symbol to distinguish them from the other sectors in this animal. *Bottom,* The same data plotted as a function of capillary volume of the retina. Here, unlike the previous graphs, *solid symbols* indicate peripapillary loci. The *straight line* is the least-squares fit to the data points indicated by the *open symbols.* Its equation is $y = 0.002x + 1.78$.

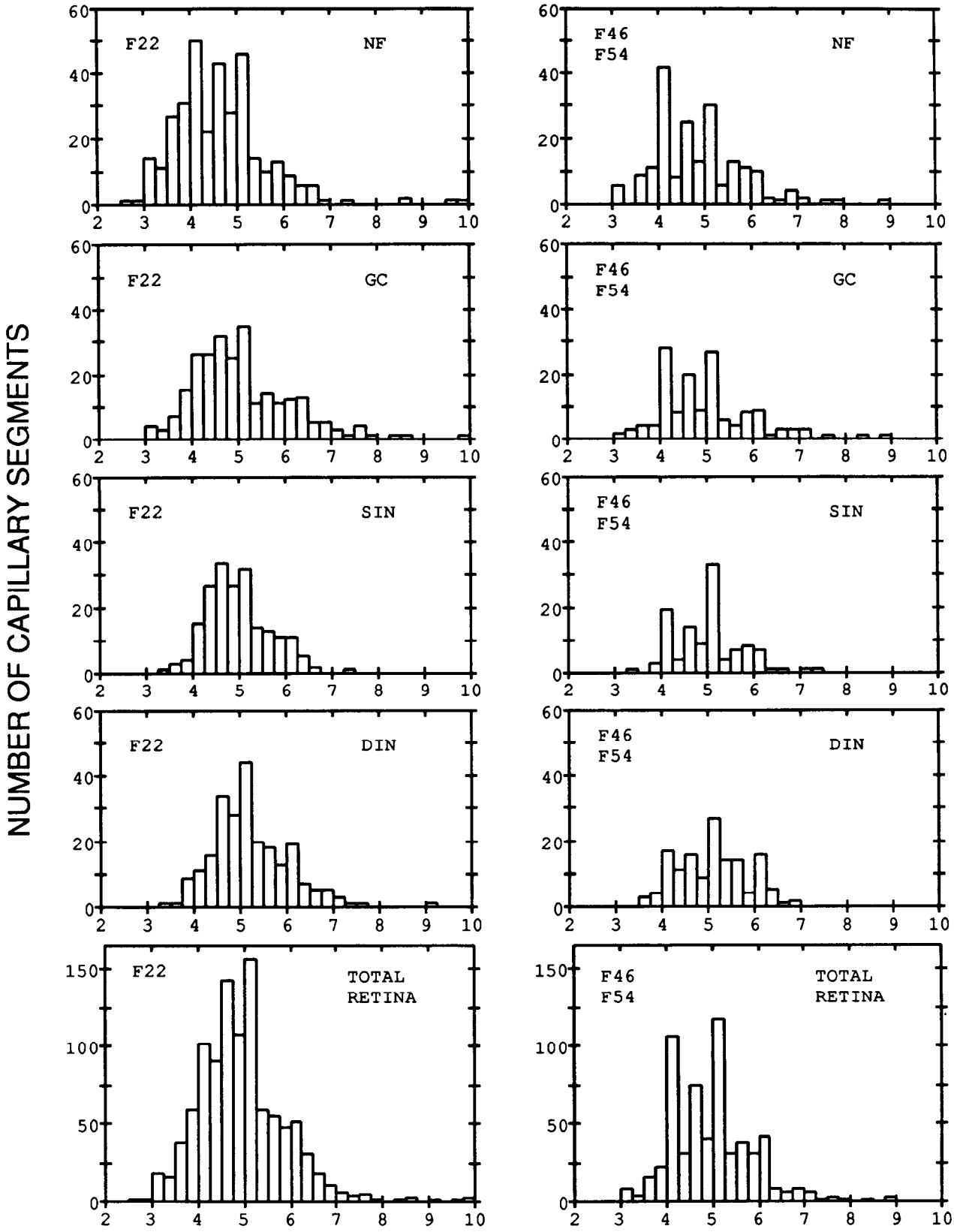
F22
NF
F46
F54
NF
F22
GC
F46
F54
GC
F22
SIN
F46
F54
SIN
F22
DIN
F46
F54
DIN
F22
TOTAL
RETINA
F46
F54
TOTAL
RETINA
NUMBER OF CAPILLARY SEGMENTS
CAPILLARY DIAMETER (μm)

cular retinas can be thicker than was previously thought (Buttery et al., 1991). Furthermore, the level of oxidative metabolism of the inner retina, as indicated by cytochrome oxidase (Wong-Riley, 1989) and malic dehydrogenase activities (Lowry et al., 1956), varies from species to species. Consequently, retinal thickness alone is not adequate to predict the oxygen demand of the retina. In seven species studied with this issue in mind, retinas with high oxidative metabolism in the inner layers have an intrinsic vascular network separate from the choroid and those with low oxidative metabolism do not (Lowry et al., 1956; Buttery et al., 1988). This is consistent with our conclusions that the metabolic characteristics of the inner retinal layers are more important than diffusion distance from the choroid in establishing retinal vascularity.

Capillary diameters and their functional implications

Capillary diameters and blood cell diameters

Since the retinal capillaries absorb and scatter the incoming photons (Snodderly and Weinhaus, 1990), one might expect that there would be selection pressure to keep capillary diameters to a minimum. In fact, the range of median luminal diameters (4.5–5.2 μm) in the capillary planes of macaque retina is quite similar to the range of mean values from microvascular networks in brain, intestine, and various muscles (Wiedeman, 1984). In most microvascular networks, including those of the central retina, the capillary diameters are sufficiently small that the blood cells must deform to pass through them in single file (Fung, 1978a,b; Cokelet, 1987; Schmid-Schonbein, 1987). An exception to this rule may occur in the far peripheral retina, where qualitative observations indicate that the vessels are larger in diameter (Spitznas and Bornfeld, 1977). However, some numerical data supporting this trend are based on human retinas obtained as much as 3 d post-mortem and then subjected to harsh histological procedures (Schroder et al., 1990). It would be useful to have data taken under more favorable conditions before attempting to interpret these findings.

Although the blood cells of monkeys have not been studied in the same detail as those of humans, they appear to be only slightly smaller. A typical value for red blood cell volume in humans is 97.9 femtoliters (fl), with a diameter of 7.65 μm for the free-floating biconcave disk (Fung, 1978a). Monkeys show species differences in the sizes of their blood cells; those with larger body size have larger blood cells (Huser, 1970). The mean red cell volume is estimated from packed cell volumes as 66.3 fl for *Macaca fascicularis* and 64.9 fl for squirrel monkeys, *Saimiri sciureus* (Huser, 1970). Data from Coulter counter sizing of cell volumes indicate that the published values for squirrel monkeys may be about 10% high (R. S. Weinhaus and D. M. Snodderly, unpublished observations). If we assume that the shape of the human red cell is scaled down to these volumes while maintaining constant ratios of its dimensions, the diameter of the biconcave disk would be about 7.1 μm and 6.8 μm for *M. fascicularis* and *S. sciureus*, respectively. These values are consistent with the diameter of 7.2 μm reported from blood smears for *M. nemestrina* (Rahlmann et al., 1967).

A lower limit on the capillary diameter is set by the elastic limits of red blood cells (Caro et al., 1978). If human red cells are forced through pores smaller than 3 μm, they rupture and hemolyze (Chien et al., 1971). Since monkey red blood cells are smaller than those of humans, the diameters of the retinal capillaries exceed minimum pore size by a comfortable margin (Fig. 14).

The blue field entoptic phenomenon

The small diameter of the retinal capillaries, causing single-file flow and deformation of blood cells, suggests the following interpretation of the striking entoptic percept that occurs when a uniform blue field is viewed. With illumination of 430 nm, the leukocytes in retinal capillaries are said to appear as moving "dotlike luminous corpuscles with a darker tail" (Riva and Petrig, 1980). In fact, the leukocytes, being more voluminous than the red blood cells, are temporarily trapped in the capillaries and distorted into a cylindrical shape (Schmid-Schonbein, 1987). When they are driven through the capillaries by each pressure pulse of the heartbeat (Riva and Petrig, 1980), they appear wormlike rather than dotlike because of their elongation (R. I. Land and D. M. Snodderly, unpublished observations).

Since the leukocytes temporarily retard flow in the capillary, a plasma gap with a lower hematocrit develops downstream and red blood cells forming a higher hematocrit accumulate upstream (Schmid-Schonbein, 1987). Remarkably, the entoptic percept appears to incorporate all these features. The dark tail is presumably the upstream accumulation of red cells, which strongly absorb the blue light. The luminous worm should include the plasma gap and the elongated body of the leukocyte, both of which are relatively transparent to the light. According to this interpretation, the entoptic "worms" should be longer than would be predicted from the diameters of the capillaries and the volumes of the leukocytes because of the plasma gap. This prediction, which is consistent with our preliminary observations (Land and Snodderly, unpublished observations) can be tested rigorously in the future.

Potential implications for disease processes

It has been suggested that part of the pathophysiology of diabetes and inflammatory disorders could be partial occlusion of small capillaries so that blood cells cannot pass through them (Ben-Nun et al., 1990). The smaller diameter of capillarics in the nerve fiber layer may imply differential vulnerability to such disease processes. In addition, it may be worthwhile to investigate the possibility that elevated intraocular pressure or other factors leading to glaucoma and nerve fiber damage could preferentially reduce flow in smaller capillaries and selectively compromise the nerve fiber layer. We hope that our more systematic understanding of neural–vascular relationships will eventually make it possible to predict whether some neural subsystems should be more vulnerable than others to disturbances of the circulation.

←

Figure 14. Histograms depicting distributions of capillary diameters. *Left column,* Data pooled from all sampling areas of F22. *Right column,* Data pooled from all sampling areas of both F46 and F54. *First four rows,* Distributions of capillary diameters in networks at different depths within the retina. Abbreviations are as in previous figures. *Bottom row,* Distribution of capillary diameters for the total retina. Statistical parameters of the distributions are listed in Table 1.

Retinal metabolism and vascularity

For those species with a well-developed retinal circulation, a growing body of physiological evidence indicates that the choroidal and retinal circulations have relatively independent roles. It is generally accepted that the choroidal circulation serves primarily the photoreceptors whereas the retinal circulation serves the inner retina (Bill, 1984; Saari, 1987).

The most time-critical function of the circulation is to supply oxygen (Linsenmeier, 1990). Studies of cat retinas show that in the dark, oxygen tension in the retina is highest near the choroid, passes through a minimum at an intermediate retinal depth, and then rises again in the inner retina (Alder et al., 1983; Linsenmeier, 1986). The location of the minimum oxygen tension is assumed to be the dividing line where oxygen is supplied primarily by the choroidal circulation on one side and by the retinal circulation on the other (Alder and Cringle, 1990). The anatomical location of the oxygen minimum has been tentatively assigned by different authors to the outer nuclear layer (Linsenmeier, 1986) or to the inner nuclear layer (Alder et al., 1983). Our results showing that the inner nuclear layer is richly vascularized are more consistent with a location of the minimum near the outer nuclear layer.

Where retinal oxygen tension reaches its minimum, it is near zero in the dark (Linsenmeier, 1986), which implies at least a partial dependence on anaerobic metabolism (Saari, 1987). Appropriately, lactic acid dehydrogenase, an enzyme associated with anaerobic glycolysis, is maximal near the vitread (shallow) border of the outer nuclear layer in monkey retinas (Lowry et al., 1956). In fact, its distribution is complementary to that of the oxidative metabolic enzymes of the mitochondria, malic dehydrogenase (Lowry et al., 1956) and cytochrome oxidase (Kageyama and Wong-Riley, 1984). The picture that emerges is an intricate interleaving of metabolic compartments, with anaerobic metabolic machinery filling in the gap between the dual vascular systems that supply the retina.

There may also be other metabolic adaptations associated with the profile of oxygen tension in the retina. For example, two pigments with spectral properties similar to respiratory hemoproteins are present in the region of the outer nuclear layer (Snodderly et al., 1984), which is near the oxygen minimum.

Like the retina, other laminated structures of the CNS have intricate complementary profiles of the enzymes for aerobic and anaerobic glucose utilization (Borowsky and Collins, 1989), but quantitative information about the laminar profiles of oxygen tension appears to be lacking. The relative accessibility of the retina, its simple geometry, and the ease of stimulating it offer the opportunity to understand relationships between the metabolism and the vasculature that would be more difficult to study in many other neural structures.

References

Alder VA, Cringle SJ (1990) Vitreal and retinal oxygenation. Albrecht Von Graefes Arch Klin Exp Ophthalmol 228:151–157.

Alder VA, Cringle SJ, Constable IJ (1983) The retinal oxygen profile in cats. Invest Ophthalmol Vis Sci 24:30–36.

Anderson DR (1971) The retinal capillary bed at the posterior pole of primate eyes. Am J Ophthalmol 71:815–818.

Bar T (1980) The vascular system of the cerebral cortex. Adv Anat Embryol Cell Biol 59:1–65.

Ben-Nun J, Alder VA, Constable IJ, Roberts CE (1990) The patency of the retinal vasculature to erythrocytes in retinal vascular disease. Invest Ophthalmol Vis Sci 31:464–470.

Bill A (1984) Circulation in the eye. In: Handbook of physiology, Sec 2, The cardiovascular system, Vol IV, Microcirculation, Pt 1 (Renkin EM, Michel CC, Geiger SR, eds), pp 1001–1034. Bethesda, MD: American Physiological Society.

Borowsky IW, Collins RC (1989) Metabolic anatomy of brain: a comparison of regional capillary density, glucose metabolism, and enzyme activities. J Comp Neurol 288:401–413.

Buttery RG, Weller WL, Haight JR (1988) Retinal cytochrome oxidase: a missing link in the electron transport chain? Neurosci Lett 30:S52.

Buttery RG, Hinrichsen CFL, Weller WL, Haight JR (1991) How thick should a retina be? A comparative study of mammalian species with and without intraretinal vasculature. Vision Res 31:169–187.

Caro CG, Pedley TJ, Schroter RC, Seed WA (1978) The mechanics of the circulation. New York: Oxford UP.

Chase J (1982) The evolution of retinal vascularization in mammals. Ophthalmology 89:1518–1525.

Chien S, Luse SA, Bryant CA (1971) Hemolysis during filtration through micropores: a scanning electron microscopic and hemorheologic correlation. Microvasc Res 3:183–203.

Cokelet GR (1987) The rheology and tube flow of blood. In: Handbook of bioengineering (Skalak R, Chien S, eds), pp 14.1–14.17. New York: McGraw-Hill.

Fine BS, Yanoff M (1979) Ocular histology. A text and atlas. Hagerstown, MD: Harper & Row.

Fung Y-C (1978a) Red blood cells and their deformability. In: Microcirculation (Kaley G, Altura BM, eds), pp 255–278. Baltimore: University Park.

Fung Y-C (1978b) Rheology of blood in microvessels. In: Microcirculation (Kaley G, Altura BM, eds), pp 279–298. Baltimore: University Park.

Henkind P (1967) Radial peripapillary capillaries of the retina. I. Anatomy: human and comparative. Br J Ophthalmol 51:115–123.

Huser H-J (1970) Atlas of comparative primate hematology. New York: Academic.

Iwasaki M, Inomata H (1986) Relation between superficial capillaries and foveal structures in the human retina. Invest Ophthalmol Vis Sci 27:1698–1705.

Kageyama GH, Wong-Riley MTT (1984) The histochemical localization of cytochrome oxidase in the retina and lateral geniculate nucleus of the ferret, cat, and monkey, with particular reference to retinal mosaics and on/off-center visual channels. J Neurosci 4:2445–2459.

Linsenmeier RA (1986) Effects of light and darkness on oxygen distribution and consumption in the cat retina. J Gen Physiol 88:521–542.

Linsenmeier RA (1990) Electrophysiological consequences of retinal hypoxia. Albrecht Von Graefes Arch Klin Exp Ophthalmol 228:143–150.

Lowry OH, Roberts NR, Lewis C (1956) The quantitative histochemistry of the retina. J Biol Chem 220:879–892.

Michaelson IC (1954) Retinal circulation in man and animals. Springfield, IL: Thomas.

Pawlik G, Rackl A, Bing RJ (1981) Quantitative capillary topography and blood flow in the cerebral cortex of cats: an *in vivo* microscopic study. Brain Res 208:35–58.

Quigley HA, Hohman RM, Addicks EM (1982) Quantitative study of optic nerve head capillaries in experimental optic disk pallor. Am J Ophthalmol 93:689–699.

Rahlmann DF, Pace N, Barnstein NJ (1967) Hematology of the pigtailed monkey, *Macaca nemestrina*. Folia Primatol (Basel) 5:280–284.

Riva CE, Petrig B (1980) Blue field entoptic phenomenon and blood velocity in the retinal capillaries. J Opt Soc Am 70:1234–1238.

Saari JC (1987) Metabolism and photochemistry in the retina. In: Physiology of the eye. Clinical application (Moses RA, Hart WM Jr, eds), pp 356–372. St. Louis: Mosby.

Schein SJ (1988) Anatomy of macaque fovea and spatial densities of neurons in foveal representation. J Comp Neurol 269:479–505.

Schmid-Schonbein GW (1987) Rheology of leukocytes. In: Handbook of bioengineering (Skalak R, Chien S, eds), pp 13.1–13.25. New York: McGraw-Hill.

Schroder S, Brab M, Schmid-Schonbein GW, Reim M, Schmid-Schonbein H (1990) Microvascular network topology of the human retinal vessels. Fortschr Ophthalmol 87:52–58.

Shimizu K, Ujiie K (1978) Structure of ocular vessels. Tokyo: Igaku-Shoin.

Snodderly DM, Weinhaus RS (1990) Retinal vasculature of the fovea of the squirrel monkey, *Saimiri sciureus*: three-dimensional architecture, visual screening, and relationships to the neuronal layers. J Comp Neurol 297:145–163.

Snodderly DM, Brown PK, Delori FC, Auran JD (1984) The macular pigment. I. Absorbance spectra, localization, and discrimination from other yellow pigments in primate retinas. Invest Ophthalmol Vis Sci 25:660–673.

Sperber GO, Bill A (1985) Blood flow and glucose consumption in the optic nerve, retina and brain: effects of high intraocular pressure. Exp Eye Res 41:639–653.

Spitznas M, Bornfeld N (1977) The architecture of the most peripheral retinal vessels. Albrecht Von Graefes Arch Klin Exp Ophthalmol 203: 217–229.

Toussaint D, Kuwabara T, Cogan DG (1961) Retinal vascular patterns. II. Human retinal vessels studied in three dimensions. Arch Ophthalmol 65:575–581.

Wiedeman MP (1984) Architecture. In: Handbook of physiology, Sec 2, The cardiovascular system, Vol IV, Microcirculation, Pt 1 (Geiger SR, Renkin EM, Michel CC, eds), pp 11–40. Bethesda, MD: American Physiological Society.

Wiederhold K-H, Bielser W Jr, Schulz U, Veteau M-J, Hunziker O (1976) Three-dimensional reconstruction of brain capillaries from frozen serial sections. Microvasc Res 11:175–180.

Wilson DJ, Finkelstein D, Quigley HA, Green WR (1988) Macular grid photocoagulation. Arch Ophthalmol 106:100–105.

Wise GN, Dollery CT, Henkind P (1971) The retinal circulation. New York: Harper & Row.

Wong-Riley MTT (1989) Cytochrome oxidase: an endogenous metabolic marker for neuronal activity. Trends Neurosci 12:94–101.

Zheng D, LaMantia A-S, Purves D (1991) Specialized vascularization of the primate visual cortex. J Neurosci 11:2622–2629.